Zentrum für Technomathematik
Fachbereich 3 – Mathematik und Informatik

Modelling and simulation of concrete carbonation with internal layers

Sebastian A. Meier, Malte A. Peter,
Adrian Muntean, Michael Böhm

Report 05–02

Berichte aus der Technomathematik

Report 05–02 April 2005

Modelling and simulation of concrete carbonation with internal layers

Sebastian A. Meier, Malte A. Peter, Adrian Muntean, Michael Böhm

Centre for Industrial Mathematics, FB 3, University of Bremen, Germany
e-mails: {sebam,mpeter,muntean,mbohm}@math.uni-bremen.de

Abstract

Transport and reaction of carbon dioxide with alkaline species in concrete is modelled by a closed system of ordinary and partial differential equations. Varying porosity and varying external exposure as well as nonlinear reaction rates are taken into account. Proper nondimensionalisation is introduced to pay attention to the different characteristic time and length scales. We emphasise the effects of the size of the Thiele modulus on the penetration curves. It is shown that an internal reaction layer is formed whose properties are related to the Thiele modulus. The model is tested for accelerated and natural carbonation settings and is found reliable. A discussion of the effects of different sizes of several model parameters yields information about their relevance. Special attention is paid to the effects of moisture on the whole process. For the accelerated setting, a water-production layer is observed.

Key words: Reaction-diffusion systems, concrete carbonation, fast reaction, Thiele modulus, internal layer, moisture transport

Contents

1 Introduction **2**

2 Carbonation scenario **4**

2.1 Basic geometry and porosity 4

2.2 Properties of the reaction layer 5

2.3 On the role of moisture 6

3 Model fomulation **8**

3.1 Active species 8

3.2 Carbonation and absorption kinetics 9

3.3 Mass balances 9

3.4 Carbonation degree and carbonation depth 11

4 Numerical implementation **11**

4.1 Weak formulation 11

4.2 Nondimensionalisation 12

4.3 Numerical solution 14

5 Simulation results **14**

5.1 Simulation of an accelerated carbonation test 15
5.2 Simulation of a natural carbonation test 16
5.3 Effects due to the variation of model parameters 21
5.3.1 Thiele modulus 21
5.3.2 CO_2-absorption coefficient 24
5.3.3 External exchange coefficient for CO_2 24
5.4 Effect of moisture 29
5.4.1 Moisture as a given constant 29
5.4.2 Moisture as a solution of a PDE 29
5.4.3 Effects of periodic moisture inputs 31
5.5 Effects of time-dependent porosity 33

6 Summary and Discussion **35**

1 Introduction

Steel bars in reinforced concrete are protected from corrosion by a microscopic oxide layer on their surface. This passive layer is maintained in a highly alkaline environment (pH $\approx$ 14). As soon as the pH level decreases, the protection from corrosion ceases and the steel bars can corrode. Consequently, the rusting of the reinforcement usually leads to a severe reduction of the durability of the structure. The main process that destroys the protection by alkalinity is *concrete carbonation*. This is one of the physicochemical processes that can indirectly but drastically limit the lifetime of reinforced concrete structures by allowing aggressive species to attack the unprotected bars. Detailed surveys and literature accounts on the carbonation problem and related aspects concerning the durability of concrete can be found, for instance, in [Bie88, Kro95, Cha99, MIK03] and [Sis04], and references therein.

The present paper is concerned with the modelling and numerical investigation of specific aspects of the concrete carbonation problem. One of the main problems in the modelling of the *overall* carbonation process are the several characteristic time and length scales. We therefore perform a nondimensionalisation of the entire model in section 4.2 and investigate the roles of several relevant parameters (cf. section 5.3). The second issue we are studying numerically is the role of moisture (cf. section 5.4). It is not yet completely understood in which way the water produced by carbonation and the exposure conditions affect the carbonation process (cf. [Cha99], e.g.). Typical questions are: Is the water produced by carbonation slowing down the CO_2 penetration into the material in a relevant way? Under which conditions does this happen? Can the moisture be treated analogously in accelerated carbonation tests, compared to natural carbonation? We rely on our simulation results to give partial answers to these and some more related questions (see dicussion in section 2.3). The third topic that we cover is the effect of a time-dependent porosity (cf. section 5.5). We particularly show effects of decreasing porosity on the carbonation process.

The carbonation process can be assumed to be solely determined by the reaction mechanism

$$\mathrm{CO_2}(g \to aq) + \mathrm{Ca(OH)_2}(s \to aq) \to \mathrm{CaCO_3}(aq \to s) + \mathrm{H_2O}, \tag{1.1}$$

accompanied by molecular diffusion of (almost) all participating species. A short summary of this scenario is the following: The atmospheric carbon dioxide diffuses through the unsaturated concrete matrix, dissolves in the pore water via a Henry-like transfer mechanism, and then reacts in the presence of water with calcium hydroxide. The latter species is available in the pore solution by dissolution from the solid matrix. Free water and calcium carbonate are the main products of reaction. Once it is built up, calcium carbonate precipitates quickly to the solid matrix. Due

to the change in the molar volumes of $Ca(OH)_2$ and $CaCO_3$ and the difference in the respective densities, the clinging of the precipitated carbonates on pore walls may lead to a decrease in the concrete porosity. While this seems to be the case for concretes with ordinary Portland cement (see [Kro83, Bie88, IMS04, SN97], e.g.), such a decrease might not happen in case of concretes with fly ash or with blast furnance (cf. [PVF91, PVF92], e.g.).

Experimental evidence (see [PVF89], e.g.) shows that the characteristic time scales of carbonation, precipitation and dissolution reactions are of strongly different magnitude, and hence, different significance when compared to the characteristic diffusion time of $CO_2(g)$. In particular, the carbonation reaction is usually much faster than diffusion of CO_2. This implies that wherever CO_2 and $Ca(OH)_2$ coexist, the carbonation reaction depletes both of them rapidly until only one is left. The continued reaction relies on dissolution of $Ca(OH)_2$ and on molecular diffusion to supply the reactants to the reaction zone. Therefore, the bulk of the reaction is usually located on a narrow internal *reaction layer* which is formed initially and progresses afterwards into the material (see also section 2.2). Thereby it separates spatially the two reactants and also the *carbonated* from the *uncarbonated part* of the concrete. Note that in pure reaction-diffusion settings, such layers can be obtained as mathematical limit-cases (cf. [Mai99, BS00], e.g.). The nondimensionalisation of the model (cf. section 4.2) can give a meaning to the notions *fast* and *slow* and yields information about the determining parameters. One of the key dimensionless numbers in this setting is the *Thiele modulus* which is the ratio between a *characteristic time of the carbonation reaction* and a *characteristic diffusion time*. For similar settings, the reader is referred to [IW68, FB90, WD96], e.g. It is pointed out numerically that the size of the Thiele modulus has strong influence on the dynamics of the reaction layer. Additionally, we show the influence of other important dimensionless quantities. In particular we focus on the interfacial mass transfer coefficients for internal (microscopic) phase boundaries as well as for the exposed (macroscopic) boundary, which are generally unknown. It is shown that the time needed in order to permit the transfer of CO_2 from the gas phase into the pore water may facilitate a sharpening or spreading of the carbonation reaction layer (cf. section 5.3).

The presence of several relevant characteristic time and length scales makes the carbonation model similar to the reaction-diffusion problem investigated in [SGS04, SGS05], e.g. In [Ort94] a large spectrum of pattern formation scenarios is listed, which arise in geochemistry and present similar phenomenological features as our problem. For related modelling in the framework of gas-solid reactions we refer to [BS00, IW68] and [SES76], e.g. It should be noted that the occurrence of a moving internal reaction layer in the concrete sample has been postulated in the earlier moving-interface carbonation models, i.e. the moving sharp-interface case (cf. [BKM03b, MB04b]), the moving layer model (cf. [BKM03b, MB04a]), and the moving two-reaction-zones situation (cf. [BKM03a, GM03]). Details on the modelling as well as on the analysis and simulation of concrete carbonation via moving boundary approaches can be found in [Mun05]. For related modelling in the context of SO_2-attacks in concrete we refer to [TM03, BDJR98, ADDN04], e.g.

The paper is organized as follows: In section 2 we describe the considered carbonation setting. We discuss the changing porosity, the dynamics of the reaction layer and the role of moisture. Additional questions are posed which are of special interest for our numerical tests. In section 3, the mathematical model of the whole process is formulated. We describe the reaction and absorption kinetics and list the mass balances of the active species, including the boundary and initial conditions. Afterwards, an appropriate definition of the carbonation degree and carbonation depth is given. Section 4 presents the variational formulation of the model on which the numerical implementation is based as well as the nondimensionalisation procedure. We shortly describe how the system is numerically solved in one space dimension. In section 5 we formulate our testing strategy, discuss the simulation results, and comment on them. This is the largest part of this paper. We simulate an accelerated carbonation test as well as a natural carbonation scenario (cf. sections 5.1 and 5.2), using data from [PVF89], and [Wie84], respectively. In sections 5.3 – 5.5, the effects of different sizes of relevant parameters, of moisture, and of the time-dependent porosity are discussed. Finally, we summarise the simulation results and conclusions in section 6.

2 Carbonation scenario

2.1 Basic geometry and porosity

We focus on a part of a concrete member which is exposed to ingress of gaseous CO_2 and humidity from the environment. Fig. 1a shows a typical structure under *natural exposure conditions*. It is assumed, for symmetry reasons, that the effects which are mainly relevant for carbonation can be captured by considering only box A. We denote by Ω the part of the concrete sample contained in box A, for which we model the carbonation process. If we refer to an *accelerated test*, then the geometry we have in mind is depicted in Fig. 1b and Ω is now part of box B. The dark area points out a zone or a very thin front of steep change in pH. This is the layer where the bulk of the reaction is located. Denoting the time variable by t, $\Omega_2(t)$ denotes the *uncarbonated zone*, $\Omega_1(t)$ is the *carbonated zone* in both figures 1a and b. The latter two notations will not be used in the sequel. Note that in both cases we are given parts of the boundary which are exposed to the environment and parts which are not.

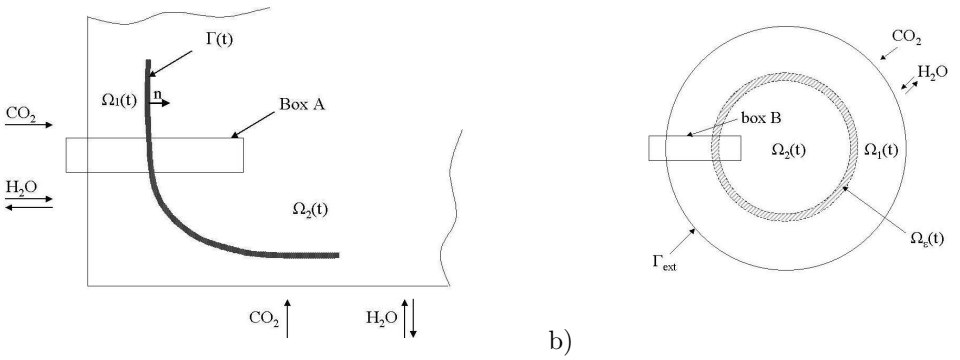

Figure 1: a) Typical corner of a concrete structure. The box A is the region which our model refers to when dealing with *natural exposure conditions*. b) Cross section of a cylindrical concrete sample. The box B is the region which our model refers to when discussing the *accelerated carbonation test*.

We introduce some concepts usually needed to describe reactive processes taking place in porous media. The region Ω is composed of the solid matrix Ω^{s} and of the totality of pore voids Ω^{p}. Furthermore, since the pore space is unsaturated and carbonation is a heterogeneous process, Ω^{p} splits into Ω^{a} (the parts filled with dry air and water vapors) and Ω^{w}(the parts filled with liquid water). By the volumetric ratio $\phi := |\Omega^{\mathrm{p}}|/|\Omega|$ we denote the concrete porosity and by $\phi^j := |\Omega^j|/|\Omega^{\mathrm{p}}|$ the air and water fractions, where $j \in \{\mathrm{a}, \mathrm{w}\}$. Regarding the evolution of ϕ we account for the following two cases:

- *Constant concrete porosity*: The initial porosity, which we denote by ϕ_0, does not change during the course of carbonation. It can be calculated as

$$\phi_0 := \frac{R_{\mathrm{w/c}} \frac{\rho_{\mathrm{c}}}{\rho_{\mathrm{w}}}}{\left(R_{\mathrm{w/c}} \frac{\rho_{\mathrm{c}}}{\rho_{\mathrm{w}}} + R_{\mathrm{a/c}} \frac{\rho_{\mathrm{c}}}{\rho_{\mathrm{a}}} + 1 \right)}, \tag{2.1}$$

  where $R_{\mathrm{w/c}}$ and $R_{\mathrm{a/c}}$ represent the water-to-cement and aggregate-to-cement ratios, while ρ_{a}, ρ_{w} and ρ_{c} are aggregate, water and concrete densities, respectively (cf. [PVF89]). Relation (2.1) is used to simulate both accelerated and natural carbonation scenarios.

- *Time-dependent concrete porosity*: In ordinary Portland cements (OPC), a decrease of pore volume due to carbonation is to be expected [Kro83, Bie88]. To capture this effect, we suggest

the following law to model the concrete porosity:

$$\phi(t) := \phi_0 \mathrm{e}^{-\alpha t/T} \qquad \text{for each } t \geq 0. \tag{2.2}$$

Here, T is a characteristic time scale and ϕ_0 is the initial concrete porosity (2.1) before the carbonation takes place. The factor α is a material parameter that usually depends on the reaction kinetics and on the differences between the molar volumes occupied by the two reactants. In our context, we have $\alpha \approx \beta\eta_{\min}$, where $\eta_{\min}$ represents a non-trivial lower bound of the carbonation kinetics and

$$\beta := \frac{m_{\mathrm{Ca(OH)_2}}}{\rho_{\mathrm{Ca(OH)_2}}} - \frac{m_{\mathrm{CaCO_3}}}{\rho_{\mathrm{CaCO_3}}} \approx -4.19\,\mathrm{cm}^3/\mathrm{mole}.$$

Here, m_ν and ρ_ν are molar mass and mass density of the species ν (cf. table 3 in the appendix). A derivation of (2.2) via first principles is performed in [Mun05].

Note that in the literature some linear alternatives to (2.2) can be found. See, e.g., [SON90, PVF89, Cha99, PVF91]. Nevertheless, the majority of simulations approaches of the carbonation model account for a constant porosity scenario, cf. [SSV95, SV04, Ste00], e.g. We assume the porosity as time-dependent, but *a priori* prescribed. In further work we plan to address the problem of a dynamical, space- and time-dependent porosity. At this moment such a working hypothesis would unnecessarily complicate the model.

2.2 Properties of the reaction layer

It is well-known from experimental observations that the carbonation reaction is located on a relatively thin zone, compared to the thickness of the concrete sample.[1] This *reaction layer* separates the carbonated from the uncarbonated zone. It can be either modelled as a relatively thin layer, or as a surface. In case of moving-interface carbonation models (see [BKM03b, BKM03a, Mun05]) the layer or front, where the carbonation reaction is located, moves with a velocity given by *a priori* prescribed *nonlocal* dynamic laws. In contrast to these formulations, in the present framework of isoline models such laws are not needed. Here a reaction layer is formed and moves *naturally*, as can be observed in our numerical simulations. Obviously, in this context, the position of the *carbonation front* or *penetration depth* should somehow express the position of the reaction layer. Unlike the moving-interface carbonation models, we have to *define* this position by means of the concentration profiles. Since we are dealing with reaction strengths of various sizes, we expect that the width of the reaction layer varies correspondingly. Therefore, a precise definition is an important issue, see section 3.4.

The dynamics of the reaction layer are determined by a *feedback mechanism* between the reaction effects and diffusion. A reaction layer is formed and moves due to a *natural* combination of some of the following facts:

(a) The reactants are initially separated.

(b) The reaction is fast compared to the diffusion of $\mathrm{CO_2}(g)$, i.e. the diffusion of $\mathrm{CO_2}(g)$ controls the reaction evolution. For quantifying this statement, we employ the notion of the *Thiele modulus* Φ^2 in section 4.2. This is a dimensionless number already used in [PVF89, FB90, WD96, Mun05], e.g. The fast regime of the reaction is described by $\Phi^2 \gg 1$.

(c) Dissolution of $\mathrm{Ca(OH)_2}(s)$ strongly influences the carbonation mechanism.

(d) The mass transfer coefficients in the Robin boundary conditions and in the production terms by Henry's law have *suitable* sizes.

[1] The carbonation penetration in the interior of a concrete sample is usually determined by *phenolphthalein tests*, see [PVF89, Wie84, Cha99, Eur98], e.g.

Although the physicochemical reasons leading to the layer's formation seem to be known, the way in which (a) – (d) combine such that this pattern is created remains unknown. With respect to the latter aspect, let us inquire about some extreme layer behaviours and expected outcomes.

(1) *Formation and approximate dynamics of the reaction layer*

   (a) The layer is not yet formed.

   (b) The layer is formed but it does not move.

   (c) The layer is formed and advances into the material; this is the case which covers most of the practical situations.

   (d) The layer position reaches some natural bound, for instance, the end of the concrete structure.

(2) *Does a spreading or a sharpening of the reaction layer occur?* If the boundary data and parameters are *uniform* we expect that for a given range of data the layer reaches an almost constant width at large times. However, some of the parameters (e.g. the mass transfer coefficient C^{ex} in the absorption terms for CO_2) may facilitate the spreading or sharpening of the layer. Inhomogeneous material properties are also supposed to produce variations in the layer's width.

(3) *Can the layer stop advancing before the whole sample is carbonated?* Under which conditions can this happen? In reality, carbonation can stop if a partial or complete carbonation-induced clogging of the pores occurs. Another possible reason can be a filling of the pores with water from the ambient atmosphere or produced by carbonation. These aspects are discussed in the preceding section.

(4) *Can we obtain some information on the velocity of the layer in spite of the fact that* we do not have *any explicit law to describe this?* An answer can be given at least in the following ways:

   (a) *asymptotically*: A way to to do this can rely upon a pseudo-steady state approximation like in Papadakis *et al.* [PVF89], or upon a *diffusive* asymptotic front penetration as suggested by Bazant and Stone [BS00] or by Mainguy [Mai99], e.g.

   (b) *empirically*: See [Sis04], table 2.2, pp. 30–31, for a collection of *semi-empirical* $\sqrt{t}$-like laws which are based on fitting arguments.

   (c) a suitable combination of (a) and (b).

   Clearly, the use of a law based on (a), (b), or (c) simplifies matters considerably! The main drawback is that they usually lose accuracy when they are applied to *different* carbonation scenarios with variable or complicated exposure conditions. Moreover, it is not very clear whether such an approximative law can encorporate correctly the effect of moisture variations. See the comments by Chaussadent on these aspects in [Cha99].

2.3 On the role of moisture

Moisture plays a very important role in what the physicochemical properties of the concrete-based materials are concerned, cf. [Kro95, Tay97, Cha99], e.g. Water appears in the pores in several phases such as vapor, mobile (liquid) water, gel water etc. It affects the transport properties (by altering the water fraction ϕ^{w}, and hence the effective diffusivities, e.g.) as well as the reaction mechanisms (the strength of the carbonation reaction depends on the local humidity, e.g.).

We address the following issues:

(1) The initial water-to-cement (w/c) ratio influences the concrete density and porosities and hence, the model properties.

(2) The influence of moisture on the carbonation reaction; we adopt *improved* carbonation reaction kinetics to account for this effect.

(3) The effect of moisture on the transport properties of $CO_2(g)$, e.g.

(4) The effect of a mass-balance equation for total humidity, in contrast to an *a priori* given humidity profile.

(5) The type of exposure (boundary) conditions.

Let us go in some detail:

(1) Water is added to the mixture of aggregate and cement to produce the hardening of the concrete sample. Note that more water is added than is actually needed by the hydration reaction to go to completion. The unhydrated water fills the pore volume and provides a favourable reactive medium for hydration, dissolution, precipitation, carbonation, etc.[2] See also [NP97, IMS04, PVF89], e.g. Additionally, the water-to-cement ratio enters into the definition of the initial concrete porosity ϕ_0, cf. eq. (2.1). See also the approach in [SN97].

(2) The carbonation reaction takes places in the pore water. Therefore, in a macroscopic model, a strong dependence of the reaction rate on the local humidity is to be expected and is also experimentally observed. This behaviour can be modelled by a modified expression for the reaction rate based on suggestions from [HRW83, SSV95, SV04, Ste00, SDA02]. See section 3.3.

(3) It is experimentally observed, that carbonation speed slows down in case of high humidity. This effect is due to a slower transport of gaseous CO_2. We will account for this effect in future work.

(4) In reality, water transport in concrete is a highly complex phenomenon, especially if it is coupled with the remaining system (for instance, via the water produced by reaction). For simplification, such couplings are often neglected. We are basically interested in the following questions: Under which conditions can such a simplification be justified? Is the water produced by reaction relevant? Partial answers to this questions are given by simulating different moisture models in section 5.4. For further discussions on these aspects we refer to [Mun05].

(5) There are several exposure scenarios. The simplest case seems to be provided by the setup of the *accelerated test*: a relative humidity (RH) of about 65% is constantly imposed in the carbonation chamber (as a Dirichlet boundary condition). The same humidity level is assumed inside the sample such that no moisture transport happens. Consequently, since diffusion, dispersion, leaching etc. cannot occur, this scenario permits the calculation of the water content which may be produced by carbonation. Note that this is only valid if the carbonation reaction can be considered decoupled from any other competitive reaction (like hydration, e.g.). On the other hand, if the concrete surface is exposed to *natural conditions*, then it is not so clear cut which boundary conditions may naturally describe the moisture inflow or outflow. It depends on the properties of the surface and atmospheric conditions at the surface. We distinguish between the following possibilities:

1. Nonperiodic inputs:
   - Various RH levels can be prescribed as Dirichlet boundary conditions.
   - The outer boundary is impermeable with respect to moisture transfer.
   - A mixture of the above cases can be well described by Robin conditions. They can also be used, for instance, to investigate the effect of a sealant on the progress of carbonation.
2. Periodic inputs:
   - A time-dependent profile can be imposed at the outer surface. Of special interest is the influence of seasonal effects which exhibit a period length of one year. Because of the small diffusivities of the species concerned, it is expected that the model output

[2] Actually, the water feeds also other reactions that compete with hydration, e.g. alkali-aggregate reactions (AAR).

is insensitive to periods like days or months. Cf. [Ste00], a periodic-like behaviour is expected for the penetration depth and carbonation degree vs. time. The main question here is whether periodic input profiles can provoke higher penetration depths than non-periodic ones, or vice versa. There is no *a priori* evidence on this issue, and therefore, such effects have to be investigated numerically.

- A profile averaged with respect to time, cf. [Arf98].

In the discussion above, we already distinguished between *accelerated* and *natural carbonation scenarios*. In fact, it is expected that the carbonation process is not analogous in the two cases (cf. [IMS04], e.g.). Differences in the results are particularly attributed to moisture distribution under different drying or wetting periods[3] as well as carbonation-induced changes in the concrete porosity. We also address this question by numerical comparisons.

3 Model fomulation

3.1 Active species

We define the active concentrations (in grams per cm^3) by:

$c_{CO_2(g)}$	–	the mass concentration of CO_2 in the air phase,
c_{CO_2}	–	the mass concentration of CO_2 in the water phase,
$c_{Ca(OH)_2}$	–	the mass concentration of $Ca(OH)_2$ in the water phase,
c_{CaCO_3}	–	the mass concentration of $CaCO_3$ in the water phase.

All concentration are *microscopic mass concentrations*, i.e. they express the mass of the species per *phase volume*.

For *moisture*, we assume an equilibrium between the liquid and the vapor phase. Under this assumption, the total moisture can be described by a single variable (cf. [Ste00, Arf98, Gru97], e.g.). For our model, we use

w – the mass concentration of moisture in the pore space.

This concentration refers to the pore volume and encorporates both the *liquid pore water* and the *vapor* from the air-filled parts. Cf. [Arf98], e.g., the moisture transport in this variable can be modelled by a diffusion equation, assuming in a first approximation a constant diffusivity of moisture.[4]

The equilibrium with the *relative humidity* RH is given by the *sorption isotherm* $\mathrm{RH}(w)$. For a range of $\mathrm{RH} \in [50\%, 80\%]$ it can be well approximated by an affine linear function, namely

$$\mathrm{RH}(w) = a + b \cdot \phi_0 \cdot w \tag{3.1}$$

The values of a and b are fitting parameters from [Ste00], see table 3 in the appendix. Note that a and b generally depend on porosity. Here, we assume them to be constant.

Note that in reality there are some other chemical substances which can get involved in the carbonation process. This depends on the particular chemical composition of the cement. For example, the calcium-silicate-hydrate (CSH)-phases can also react with CO_2 (cf. [PVF89]). We account for a more complex chemistry in [PMMB05].

[3] Cf. R. Breitenbücher, personal communication (A.M.) at the conference in Bochum, ICLODC 2004. See also [IMS04], section 5, and [Cha99].

[4] It is worth noting that the diffusion coefficient for moisture may have drastically different values for low moisture compared with very wet ones. Nevertheless we expect reasonable results for relative humidities between approx. 50% and 80%.

3.2 Carbonation and absorption kinetics

We consider the carbonation kinetics described by power-law kinetics having an *improved* reaction constant. We define the reaction rate in moles/(day $\cdot$ cm^3) as

$$\eta := C^{\mathrm{reac}} f^{\mathrm{hum}}(w) c_{\mathrm{CO_2}}^p c_{\mathrm{Ca(OH)_2}}^q. \tag{3.2}$$

Here, C^{reac} is the reaction constant for carbonation. For the exponents p, q, we assume $p, q \geq 1$. The factor $f^{\mathrm{hum}}(w)$ is defined as

$$f^{\mathrm{hum}}(w) := g^{\mathrm{hum}}(\mathrm{RH}(w)). \tag{3.3}$$

RH is the relative humidity calculated from w, cf. (3.1). The *humidity factor* describes the dependence of the carbonation kinetics on RH. According to [Ste00, SSV93], (3.3) can be written as

$$g^{\mathrm{hum}}(\mathrm{RH}) = \begin{cases} 0, & \mathrm{RH} \leq 0.5, \\ 5/2(\mathrm{RH} - 0.5), & 0.5 < \mathrm{RH} \leq 0.9, \\ 1, & \mathrm{RH} > 0.9. \end{cases} \tag{3.4}$$

One of the remaining issues is a proper identification of the (temperature-dependent) Arrhenius constant C^{reac}. We are only aware of a few references where possible values for this constant are mentioned ([Ste00, IM01, Cha99], e.g., in case of a first-order kinetics w.r.t. CO_2).

For each species $\nu \in \{\mathrm{CO_2}, \mathrm{Ca(OH)_2}, \mathrm{CaCO_3}, \mathrm{H_2O}\}$, expression (3.2) multiplied by the molar mass m_ν yields a production term given by

$$f_\nu^{\mathrm{reac}} := m_\nu C^{\mathrm{reac}} f^{\mathrm{hum}}(w) c_{\mathrm{CO_2}}^p c_{\mathrm{Ca(OH)_2}}^q. \tag{3.5}$$

Finally, we assume the production term due to absorption of $CO_2(g)$ to have the form

$$f^{\mathrm{Henry}} := C^{\mathrm{ex}}(C^{\mathrm{Henry}} c_{\mathrm{CO_2}(g)} - c_{\mathrm{CO_2}}). \tag{3.6}$$

Here, C^{Henry} denotes the dimensionless Henry constant and C^{ex} is a macroscopic mass transfer coefficient for CO_2.

3.3 Mass balances

We formulate the macroscopic mass balances for CO_2 in air and liquid phase and for $Ca(OH)_2$ and $CaCO_3$ in the liquid phase, whereas the moisture balance is formulated in the whole pore space. Detailed descriptions of some of the modelling aspects can be found in [BKM03b, BKM03a, Mun05].

In what follows, Ω stands for the concrete sample under consideration (cf. section 2.1). Its geometric boundary is denoted by Γ. This boundary splits into a part Γ^{R} which is exposed to the environment and an interior part Γ^{N} which is not exposed (cf. figure 1). The outward unit normal to Γ is denoted by the vector ν. The underlying time interval is $S := (0, T_{\max})$. The initial and ambient concentrations of species ν are denoted by c_ν^0 and c_ν^{ext}, respectively. See also table 3 in the appendix for a list of parameters.

Mass balance for $CO_2(g)$:

$$\begin{aligned} &\partial_t\big(\phi(t)\phi^{\mathrm{a}}(t) c_{\mathrm{CO_2}(g)}(x,t)\big) - \nabla \cdot \big(D_{\mathrm{CO_2}(g)}\phi(t)\phi^{\mathrm{a}}(t)\nabla c_{\mathrm{CO_2}(g)}(x,t)\big) \\ &\qquad = -f^{\mathrm{Henry}}(x,t), \qquad x \in \Omega,\, t \in S, \end{aligned} \tag{3.7a}$$

$$-\big(D_{\mathrm{CO_2}(g)}\phi(t)\phi^{\mathrm{a}}(t)\nabla c_{\mathrm{CO_2}(g)}(x,t)\big) \cdot \nu = 0, \qquad x \in \Gamma^{\mathrm{N}},\, t \in S, \tag{3.7b}$$

$$\begin{aligned} &-\big(D_{\mathrm{CO_2}(g)}\phi(t)\phi^{\mathrm{a}}(t)\nabla c_{\mathrm{CO_2}(g)}(x,t)\big) \cdot \nu \\ &\qquad = C^{\mathrm{Rob}}_{\mathrm{CO_2}(g)}(c_{\mathrm{CO_2}(g)}(x,t) - c^{\mathrm{ext}}_{\mathrm{CO_2}(g)}(x,t)), \qquad x \in \Gamma^{\mathrm{R}},\, t \in S, \end{aligned} \tag{3.7c}$$

$$c_{\mathrm{CO_2}(g)}(x,0) = c^0_{\mathrm{CO_2}(g)}(x), \qquad x \in \Omega. \tag{3.7d}$$

Mass balance for $CO_2(aq)$:

$$\begin{aligned}\partial_t\big(\phi(t)\phi^{\mathrm{w}}(t)c_{\mathrm{CO_2}}(x,t)\big) - \nabla\cdot\big(D_{\mathrm{CO_2}}\phi(t)\phi^{\mathrm{w}}(t)\nabla c_{\mathrm{CO_2}}(x,t)\big)\\ = f^{\mathrm{Henry}}(x,t) - \phi(t)\phi^{\mathrm{w}}(t)f^{\mathrm{reac}}_{\mathrm{CO_2}}(x,t), \qquad x\in\Omega,\, t\in S,\end{aligned} \tag{3.8a}$$

$$-\big(D_{\mathrm{CO_2}}\phi(t)\phi^{\mathrm{w}}(t)\nabla c_{\mathrm{CO_2}}(x,t)\big)\cdot\nu = 0, \qquad x\in\Gamma,\, t\in S, \tag{3.8b}$$

$$c_{\mathrm{CO_2}}(x,0) = c^0_{\mathrm{CO_2}}(x), \qquad x\in\Omega. \tag{3.8c}$$

Mass balance for $Ca(OH)_2$:

$$\begin{aligned}\partial_t\big(\phi(t)\phi^{\mathrm{w}}(t)c_{\mathrm{Ca(OH)_2}}(x,t)\big) - \nabla\cdot\big(D_{\mathrm{Ca(OH)_2}}\phi(t)\phi^{\mathrm{w}}(t)\nabla c_{\mathrm{Ca(OH)_2}}(x,t)\big)\\ = -\phi(t)\phi^{\mathrm{w}}(t)f^{\mathrm{reac}}_{\mathrm{Ca(OH)_2}}(x,t), \qquad x\in\Omega,\, t\in S,\end{aligned} \tag{3.9a}$$

$$-\big(D_{\mathrm{Ca(OH)_2}}\phi(t)\phi^{\mathrm{w}}(t)\nabla c_{\mathrm{Ca(OH)_2}}(x,t)\big)\cdot\nu = 0, \qquad x\in\Gamma,\, t\in S, \tag{3.9b}$$

$$c_{\mathrm{Ca(OH)_2}}(x,0) = c^0_{\mathrm{Ca(OH)_2}}(x), \qquad x\in\Omega. \tag{3.9c}$$

Mass balance for moisture:

$$\begin{aligned}\partial_t\big(\phi(t)w(x,t)\big) - \nabla\cdot\big(D_{\mathrm{H_2O}}\phi(t)\nabla w(x,t)\big)\\ = \phi(t)\phi^{\mathrm{w}}(t)f^{\mathrm{reac}}_{\mathrm{H_2O}}(x,t), \qquad x\in\Omega,\, t\in S,\end{aligned} \tag{3.10a}$$

$$-\big(D_{\mathrm{H_2O}}\phi(t)\nabla w(x,t)\big)\cdot\nu = 0, \qquad x\in\Gamma^{\mathrm{N}},\, t\in S, \tag{3.10b}$$

$$-\big(D_{\mathrm{H_2O}}\phi(t)\nabla w(x,t)\big)\cdot\nu = C^{\mathrm{Rob}}_{\mathrm{H_2O}}(w(x,t) - w^{\mathrm{ext}}(x,t)), \quad x\in\Gamma^{\mathrm{R}},\, t\in S, \tag{3.10c}$$

$$w(x,0) = w^0(x), \qquad x\in\Omega. \tag{3.10d}$$

Mass balance for $CaCO_3$:

$$\begin{aligned}\partial_t\big(\phi(t)\phi^{\mathrm{w}}(t)c^{\mathrm{w}}_{\mathrm{CaCO_3}}(x,t)\big) - \nabla\cdot\big(D_{\mathrm{CaCO_3}}\phi(t)\phi^{\mathrm{w}}(t)\nabla c_{\mathrm{CaCO_3}}(x,t)\big)\\ = +\phi(t)\phi^{\mathrm{w}}(t)f^{\mathrm{reac}}_{\mathrm{CaCO_3}}(x,t), \qquad x\in\Omega,\, t\in S,\end{aligned} \tag{3.11a}$$

$$-\big(D_{\mathrm{CaCO_3}}\phi(t)\phi^{\mathrm{w}}(t)\nabla c_{\mathrm{CaCO_3}}(x,t)\big)\cdot\nu = 0, \qquad x\in\Gamma,\, t\in S, \tag{3.11b}$$

$$c_{\mathrm{CaCO_3}}(x,0) = c^0_{\mathrm{CaCO_3}}(x), \qquad x\in\Omega. \tag{3.11c}$$

Remark 3.1 *1. The diffusivities D_ν are* not *effective ones. They refer to the microscale and possibly incorporate a tortuosity factor. See [SMB99], e.g.*

2. *The overall structure of the production term by reaction corresponds to the proposals in [HRW83, SSV95, Ste00], e.g. It is worth noting that there is not a general agreement on the selection of kinetics, and that there are several more competing ways to model the carbonation reaction. See [MB04b] for a discussion on these matters. Furthermore, a preliminary investigation of the model stability, when different reaction kinetics drive partially-carbonated zones, is performed in [GM03].*

3. *At the* exposed boundary, Robin boundary conditions *are employed for $CO_2(g)$ and moisture. This enables us to account for different exposure scenarios by varying the coefficient C^{Rob}_ν. For example, a Dirichlet condition can be approximated by $C^{\mathrm{Rob}}_\nu \gg 1$.*

4. *At the* unexposed boundary Γ^{N} *we use* homogeneous Neumann boundary conditions *for all mass balances. Obviously this assumption can only be valid as long as the reaction zone is sufficiently far away from Γ^{N}. Therefore, for a given time interval $(0, T_{\max})$ under observation the domain Ω has to be choosen large enough.*

5. *For simplification in this note, we assume the volume fractions $\phi^{\mathrm{a}}(t)$ and $\phi^{\mathrm{w}}(t)$ to be* a priori *given. Thus, we neglect local changes due to water transport. In a more advanced modelling setting, $\phi^{\mathrm{a}}(t)$ and $\phi^{\mathrm{w}}(t)$ will depend dynamically on w.*

6. *The correct size of the mass-transfer coefficient C^{ex} is generally not known. Therefore, we numerically examine the role of this parameter in section 5.3.2.*

3.4 Carbonation degree and carbonation depth

As discussed in 2.2, a *reaction front* within this model has to be defined *a posteriori* in terms of the concentration profiles. We first employ the notion of the *carbonation degree*. Namely, we introduce the *local degree of carbonation* as the ratio between the locally produced calcium carbonate (which in our setting equals the locally consumed calcium hydroxide, up to a positive factor) and the maximum obtainable calcium carbonate, i.e.

$$\kappa(x,t) := \frac{\phi(t)\phi^{\mathrm{w}}(t)c_{\mathrm{CaCO_3}}(x,t)}{\phi^{\mathrm{m}}\phi^{\mathrm{w,m}}c^{\mathrm{m}}_{\mathrm{CaCO_3}}} \qquad \text{for all } x \in \Omega,\ t \in S. \tag{3.12}$$

Here, ϕ^{m} and $\phi^{\mathrm{w,m}}$ are maximal values of porosity and water fraction. If diffusion of $\mathrm{Ca(OH)_2}$ in pore water is sufficiently slow, the maximal obtainable calcium carbonate concentration can be estimated by simply balancing the carbonation reaction. This leads to

$$c^{\mathrm{m}}_{\mathrm{CaCO_3}} = \frac{m_{\mathrm{CaCO_3}}}{m_{\mathrm{Ca(OH)_2}}} \cdot c^0_{\mathrm{Ca(OH)_2}} + c^0_{\mathrm{CaCO_3}}. \tag{3.13}$$

We also define the *bulk carbonation degree* by

$$\bar{\kappa}(t) := \frac{1}{|\Omega|}\int_\Omega \kappa(x,t)\,\mathrm{d}x \qquad \text{for each } t \in S. \tag{3.14}$$

Note that there are different, more or less equivalent, definitions of a carbonation degree in literature. See [SDA02], e.g.

We define the *carbonation-reaction front* to be the isoline which corresponds to a carbonation degree equal to 0.9, i.e.

$$s(t) := \{x \in \Omega \,|\, \kappa(x,t) = 0.9\} \qquad \text{for each } t \in S. \tag{3.15}$$

Analogous definitions of the carbonation front on other isolines can be found in [SSV95, SSV93], e.g. We follow here the way indicated in [Ste00, SDA02].

4 Numerical implementation

In this section, we first present a weak formulation of our model. Afterwards, we perform a nondimensionalisation of all quantities. The resulting system of equations is solved in one-space dimension by using the Galerkin Finite Element method.

4.1 Weak formulation

We formulate the system (3.7)–(3.11) in terms of macroscopic quantities. More precisely, we perform a transformation of the quantities from the previous section into volume-averaged concentrations

$$\tilde{c}_{\mathrm{CO_2}(g)} := \phi\phi^{\mathrm{a}}c_{\mathrm{CO_2}(g)}, \qquad \tilde{c}_{\mathrm{CO_2}} := \phi\phi^{\mathrm{w}}c_{\mathrm{CO_2}}, \qquad \tilde{w} := \phi w \quad \text{etc.} \tag{4.1}$$

We exclusively use the macroscopic quantities in the following, so – for ease of notation – we omit the tilde from now on. For the transformation, it has to be taken into account that $\phi = \phi(t)$, $\phi^{\mathrm{a}} = \phi^{\mathrm{a}}(t)$, and $\phi^{\mathrm{w}} = \phi^{\mathrm{w}}(t)$ can vary in time. The main advantage of this procedure is that these quantities solely appear in the production terms on the right-hand sides of the equations.

We define the function space $\mathcal{W}$ as

$$\mathcal{W} = \{v \in L^2(0,T;H^1(\Omega)) \,|\, \partial_t v \in L^2(0,T;(W^{1,2}(\Omega))')\}. \tag{4.2}$$

See [DL92], e.g., for information on Sobolev spaces.

The weak formulation of (3.7)–(3.11) is given as follows:

$$\begin{aligned} c_{\mathrm{CO_2}(g)} \in \mathcal{W}, \quad c_{\mathrm{CO_2}(g)}(0) = \phi(0)\phi^{\mathrm{a}}(0)c^0_{\mathrm{CO_2}(g)} \quad \text{such that} \\ (\partial_t c_{\mathrm{CO_2}(g)} \,|\, v)_\Omega + D_{\mathrm{CO_2}(g)}(\nabla c_{\mathrm{CO_2}(g)} \,|\, \nabla v)_\Omega \\ = -(f^{\mathrm{Henry}} \,|\, v)_\Omega - C^{\mathrm{Rob}}_{\mathrm{CO_2}(g)}(c_{\mathrm{CO_2}(g)} - \phi\phi^{\mathrm{a}} c^{\mathrm{ext}}_{\mathrm{CO_2}(g)} \,|\, v)_{\Gamma^{\mathrm{R}}} \end{aligned} \tag{4.3}$$

a.e. in S for all $v \in \mathcal{W}$,

$$\begin{aligned} c_{\mathrm{CO_2}} \in \mathcal{W}, \quad c_{\mathrm{CO_2}}(0) = \phi(0)\phi^{\mathrm{w}}(0)c^0_{\mathrm{CO_2}} \quad \text{such that} \\ (\partial_t c_{\mathrm{CO_2}} \,|\, v)_\Omega + D_{\mathrm{CO_2}}(\nabla c_{\mathrm{CO_2}} \,|\, \nabla v)_\Omega = -(f^{\mathrm{reac}}_{\mathrm{CO_2}} \,|\, v)_\Omega + (f^{\mathrm{Henry}} \,|\, v)_\Omega \end{aligned} \tag{4.4}$$

a.e. in S for all $v \in \mathcal{W}$,

$$\begin{aligned} c_{\mathrm{Ca(OH)_2}} \in \mathcal{W}, \quad c_{\mathrm{Ca(OH)_2}}(0) = \phi(0)\phi^{\mathrm{w}}(0)c^0_{\mathrm{Ca(OH)_2}} \quad \text{such that} \\ (\partial_t c_{\mathrm{Ca(OH)_2}} \,|\, v)_\Omega + D_{\mathrm{Ca(OH)_2}}(\nabla c_{\mathrm{Ca(OH)_2}} \,|\, \nabla v)_\Omega = -(f^{\mathrm{reac}}_{\mathrm{Ca(OH)_2}} \,|\, v)_\Omega \end{aligned} \tag{4.5}$$

a.e. in S for all $v \in \mathcal{W}$,

$$\begin{aligned} w \in \mathcal{W}, \quad w(0) = \phi(0)w^0 \quad \text{such that} \\ (\partial_t w \,|\, v)_\Omega + D_{\mathrm{H_2O}}(\nabla w \,|\, \nabla v)_\Omega = (f^{\mathrm{reac}}_{\mathrm{H_2O}} \,|\, v)_\Omega - C^{\mathrm{Rob}}_{\mathrm{H_2O}}(w - \phi w^{\mathrm{ext}} \,|\, v)_{\Gamma^{\mathrm{R}}} \end{aligned} \tag{4.6}$$

a.e. in S for all $v \in \mathcal{W}$, and

$$\begin{aligned} c_{\mathrm{CaCO_3}} \in \mathcal{W}, \quad c_{\mathrm{CaCO_3}}(0) = \phi(0)\phi^{\mathrm{w}}(0)c^0_{\mathrm{CaCO_3}} \quad \text{such that} \\ (\partial_t c_{\mathrm{CaCO_3}} \,|\, v)_\Omega + D_{\mathrm{CaCO_3}}(\nabla c_{\mathrm{CaCO_3}} \,|\, \nabla v)_\Omega = +(f^{\mathrm{reac}}_{\mathrm{CaCO_3}} \,|\, v)_\Omega \end{aligned} \tag{4.7}$$

a.e. in S for all $v \in \mathcal{W}$. The production terms are re-defined as

$$f^{\mathrm{Henry}} := C^{\mathrm{ex}}(C^{\mathrm{Henry}}(\phi\phi^{\mathrm{a}})^{-1} c_{\mathrm{CO_2}(g)} - (\phi\phi^{\mathrm{w}})^{-1} c_{\mathrm{CO_2}}), \tag{4.8}$$

$$f^{\mathrm{reac}}_\nu = m_\nu C^{\mathrm{reac}} f^{\mathrm{hum}}(\phi^{-1}w)(\phi\phi^{\mathrm{w}})^{1-p-q}(c_{\mathrm{CO_2}})^p (c_{\mathrm{Ca(OH)_2}})^q, \tag{4.9}$$

where $\nu \in \{\mathrm{CO_2}, \mathrm{Ca(OH)_2}, \mathrm{H_2O}, \mathrm{CaCO_3}\}$.

4.2 Nondimensionalisation

In general, it is a difficult task to find an *appropriate scaling* for a system in which numerous model parameters as well as different time and space scales are involved. Here, we only list the transformations and dimensionless parameters we are using. See [Mun05, PVF89] for some motivating ideas about choosing appropriate scalings for the carbonation process.

We define the dimensionless quantities

$$\begin{aligned} u_1 &:= c_{\mathrm{CO_2}(g))}/c^{\mathrm{m}}_1, \qquad u_2 := c_{\mathrm{CO_2}}/c^{\mathrm{m}}_2, \qquad u_3 := c_{\mathrm{Ca(OH)_2}}/c^{\mathrm{m}}_3, \\ u_4 &:= w/c^{\mathrm{m}}_4, \qquad\qquad u_5 := c_{\mathrm{CaCO_3}}/c^{\mathrm{m}}_5, \end{aligned} \tag{4.10}$$

where the c^{m}_i, $i = 1, \ldots 5$ are some *maximal concentrations*. In order to make a reasonable choice for the c^{m}_i and to simplify the model, we make the following *assumptions*:

- $c^0_{\mathrm{CO_2}(g)} = c^0_{\mathrm{CO_2}} = 0$.
- $c^{\mathrm{ext}}_{\mathrm{CO_2}(g)}$, $c^0_{\mathrm{Ca(OH)_2}}$, w^0, $c^0_{\mathrm{CaCO_3}}$ are nonnegative constants, and w^{ext} is bounded from above by the positive constant $w^{\mathrm{ext,m}}$.

- The porosity has its maximal value at the beginning, i.e. $\phi(t) \leq \phi(0)\ \forall t \in S$. This assumption is consistent with the law proposed in (2.2).
- Diffusion of the species in water is sufficiently slow compared to diffusion in air.

The maximal concentrations are defined as

$$c_1^{\mathrm{m}} := \phi(0)\phi^{\mathrm{a}}(0)c^{\mathrm{ext}}_{\mathrm{CO_2}(g)}, \tag{4.11}$$

$$c_2^{\mathrm{m}} := \phi(0)\phi^{\mathrm{w}}(0)C^{\mathrm{Henry}}c^{\mathrm{ext}}_{\mathrm{CO_2}(g)}, \tag{4.12}$$

$$c_3^{\mathrm{m}} := \phi(0)\phi^{\mathrm{w}}(0)c^0_{\mathrm{Ca(OH)_2}}, \tag{4.13}$$

$$c_4^{\mathrm{m}} := \max\left\{\frac{m_{\mathrm{H_2O}}}{m_{\mathrm{Ca(OH)_2}}}\phi(0)\phi^{\mathrm{w}}(0)c^0_{\mathrm{Ca(OH)_2}} + \phi(0)w^0,\ \phi(0)w^{\mathrm{ext,m}}\right\}, \tag{4.14}$$

$$c_5^{\mathrm{m}} := \frac{m_{\mathrm{CaCO_3}}}{m_{\mathrm{Ca(OH)_2}}}\phi(0)\phi^{\mathrm{w}}(0)c^0_{\mathrm{Ca(OH)_2}} + \phi(0)\phi^{\mathrm{w}}(0)c^0_{\mathrm{CaCO_3}}. \tag{4.15}$$

Note that (4.15) has already been introduced in (3.13) to define a carbonation degree. The definition (4.14) is based upon similar arguments.

Define a *characteristic diffusion time* for $\mathrm{CO_2}(g)$, which is the fastest species involved, as

$$T := L^2/D_{\mathrm{CO_2}(g)}.$$

Let $\tilde{t} := t/T$ and $\tilde{x} := x/L$ be the dimensionless time and space coordinates which are defined on corresponding dimensionless domains $\tilde{\Omega}$ and $\tilde{S}$. As before, we will omit the tilde in what follows.

With the above definitions we are led to the introduction of the following dimensionless quantities:

$$\begin{aligned}
&\beta_2 := \frac{c_2^{\mathrm{m}}}{c_1^{\mathrm{m}}}, \qquad \beta_3 := \frac{c_3^{\mathrm{m}} m_{\mathrm{CO_2}}}{c_1^{\mathrm{m}} m_{\mathrm{Ca(OH)_2}}}, \qquad \beta_4 := \frac{c_4^{\mathrm{m}} m_{\mathrm{CO_2}}}{c_1^{\mathrm{m}} m_{\mathrm{H_2O}}}, \qquad \beta_5 := \frac{c_5^{\mathrm{m}} m_{\mathrm{CO_2}}}{c_1^{\mathrm{m}} m_{\mathrm{CaCO_3}}}\\
&\delta_2 := \frac{D_{\mathrm{CO_2}}}{D_{\mathrm{CO_2}(g)}}, \qquad \delta_3 := \frac{D_{\mathrm{Ca(OH)_2}}}{D_{\mathrm{CO_2}(g)}}, \qquad \delta_4 := \frac{D_{\mathrm{H_2O}}}{D_{\mathrm{CO_2}(g)}}, \qquad \delta_5 := \frac{D_{\mathrm{CaCO_3}}}{D_{\mathrm{CO_2}(g)}},\\
&\Phi^2 := \frac{L^2 m_{\mathrm{CO_2}} (c_2^{\mathrm{m}})^p (c_3^{\mathrm{m}})^q}{D_{\mathrm{CO_2}(g)} c_1^{\mathrm{m}}} C^{\mathrm{reac}} \qquad (\textit{Thiele modulus}),\\
&W^{\mathrm{Hen}} := \frac{L^2}{D_{\mathrm{CO_2}(g)}} C^{\mathrm{ex}}, \quad W_1^{\mathrm{Rob}} := \frac{L}{D_{\mathrm{CO_2}(g)}} C^{\mathrm{Rob}}_{\mathrm{CO_2}(g)}, \quad W_4^{\mathrm{Rob}} := \frac{L}{D_{\mathrm{CO_2}(g)}} C^{\mathrm{Rob}}_{\mathrm{H_2O}}.
\end{aligned} \tag{4.16}$$

The quantities β_i are usually called *impact* or *capacity factors*, whereas δ_i are ratios comparing each diffusivity with that of $\mathrm{CO_2}(g)$. The *Thiele modulus* Φ^2 describes the rapidness of the carbonation reaction. The factors W^{Hen}, W_1^{Rob}, and W_4^{Rob} account for the rapidness of different types of *interfacial-mass transfer*. Typical values of these parameters are shown in tables 1 and 2 in section 5.

For notational purposes we finally set

$$\begin{aligned}
&u_1^{\mathrm{ext}} := \frac{\phi(t)\phi^{\mathrm{a}}(t)c^{\mathrm{ext}}_{\mathrm{CO_2}(g)}}{c_1^{\mathrm{m}}}, \qquad u_4^{\mathrm{ext}} := \frac{\phi(t)w^{\mathrm{ext}}}{c_4^{\mathrm{m}}},\\
&u_4^0 := \frac{\phi(0)w^0}{c_4^{\mathrm{m}}}, \qquad \text{and} \qquad u_5^0 := \frac{\phi(0)\phi^{\mathrm{w}}(0)c^0_{\mathrm{CaCO_3}}}{c_5^{\mathrm{m}}}.
\end{aligned} \tag{4.17}$$

Transformation of the system (4.3)–(4.7) into the new quantities yields the final system which is to be solved numerically:

$$\begin{aligned}
&u_1 \in \mathcal{W}, \quad u_1(0) = 0 \text{ such that}\\
&(\partial_t u_1 \,|\, v)_\Omega + (\nabla u_1 \,|\, \nabla v)_\Omega = -(f^{\mathrm{Henry}} \,|\, v)_\Omega - W_1^{\mathrm{Rob}}(u_1 - u_1^{\mathrm{ext}} \,|\, v)_{\Gamma^{\mathrm{R}}},
\end{aligned} \tag{4.18}$$

$$\begin{gathered} u_2 \in \mathcal{W}, \quad u_2(0) = 0 \text{ such that} \\ \beta_2(\partial_t u_2 \,|\, v)_\Omega + \beta_2 \delta_2 (\nabla u_2 \,|\, \nabla v)_\Omega = +(f^{\text{Henry}} \,|\, v)_\Omega - (f^{\text{reac}} \,|\, v)_\Omega, \end{gathered} \tag{4.19}$$

$$\begin{gathered} u_3 \in \mathcal{W}, \quad u_3(0) = 1 \text{ such that} \\ \beta_3(\partial_t u_3 \,|\, v)_\Omega + \beta_3 \delta_3 (\nabla u_3 \,|\, \nabla v)_\Omega = -(f^{\text{reac}} \,|\, v)_\Omega, \end{gathered} \tag{4.20}$$

$$\begin{gathered} u_4 \in \mathcal{W}, \quad u_4(0) = u_4^0 \text{ such that} \\ \beta_4(\partial_t u_4 \,|\, v)_\Omega + \beta_4 \delta_4 (\nabla u_4 \,|\, \nabla v)_\Omega = +(f^{\text{reac}} \,|\, v)_\Omega - W_4^{\text{Rob}} \beta_4 (u_4 - u_4^{\text{ext}} \,|\, v)_{\Gamma^{\text{R}}}, \end{gathered} \tag{4.21}$$

$$\begin{gathered} u_5 \in \mathcal{W}, \quad u_5(0) = u_5^0 \text{ such that} \\ \beta_5(\partial_t u_5 \,|\, v)_\Omega + \beta_5 \delta_5 (\nabla u_5 \,|\, \nabla v)_\Omega = (f^{\text{reac}} \,|\, v)_\Omega, \end{gathered} \tag{4.22}$$

where each equation has to be satisfied for a.e. $t \in S$ and for all $v \in \mathcal{W}$. The *dimensionless production terms* are

$$f^{\text{Henry}} := W^{\text{Hen}} (C^{\text{Henry}} (\phi \phi^{\text{a}})^{-1} u_1 - (\phi \phi_w)^{-1} \beta_2 u_2), \tag{4.23}$$

$$f^{\text{reac}} := \Phi^2 \cdot (\phi \phi_w)^{1-p-q} f^{\text{hum}} (u_4 c_4^{\text{m}} \phi^{-1}) u_2^p u_3^q. \tag{4.24}$$

4.3 Numerical solution

The equations (4.18)–(4.22) form a weakly-coupled system of semi-linear parabolic equations. We solve it numerically in one space-dimension by using a standard finite-element discretisation method. More precisely, we accomplish a semi-discretisation in space on a uniform mesh of width $h = 1/(n-1)$ by the Galerkin method. For the test and trial functions, first-order splines are used. In addition, we apply the standard mass-lumping scheme, cf. [KA00], e.g. See [GM03] for a more detailed description of a similar discretisation problem. The nonlinear f^{reac}-terms are approximated by the trapezoidal rule.

The resulting stiff system of $5 \times n$ odes is numerically integrated using the MATLAB ODE solver `ode15s`. This is a variable order solver based on numerical differentiation formulas (NDFs).[5]

The examples in the following section are obtained by choosing $n = 80$.

5 Simulation results

In this section, we present some results of the numerical simulations. We are particularly interested in qualitative effects caused by variation of some details of the model. In particular, we address the following issues:

- effects due to the variation of parameters which are generally unknown but are assumed to have a strong influence on the carbonation process, namely
  - the Thiele modulus,
  - the mass-transfer coefficient of CO_2-absorption,
  - the mass-transfer coefficient of CO_2 at the exposed boundary,
- effects of *different moisture models*, i.e. we compare the different scenarios
  - moisture as a given function,
  - moisture as a solution of a PDE,

  each of these with either constant or periodic inputs,

[5] See `www.mathworks.com` for details and further references.

- effects of a time-dependent porosity.

In particular we are interested in the formation and the width of the reaction layer (or reaction zone). We recall that this is the part of Ω where, at a given time t, a noticeable carbonation reaction is localised. Let $\delta > 0$ be an appropriate lower bound for the carbonation reaction rate f^{reac} given by (4.24). The reaction zone is then identified with

$$\Omega^{\mathrm{reac}}(t) := \{x \in \Omega \,|\, f^{\mathrm{reac}}(x,t) > \delta\} \qquad \text{for each } t \in S. \tag{5.1}$$

For our plots, we use $\delta := 0.01 \cdot \max\{f^{\mathrm{reac}}(x,t) \,|\, x \in \Omega,\ t \in S\}$.

In order to have a reference data set to refer to, we introduce two *standard sets* of parameters: one for an accelerated carbonation test and another one for carbonation under natural conditions. According to data taken from literature, both data sets can be thought of as in the *correct range* with respect to the respective concrete carbonation problem. The standard sets of parameters are listed in the appendix (table 4). Particularly, we choose $p = q = 1$ in the reaction rates and $D_{\mathrm{CaCO_3}} = 0$ in both cases. However, the model allows for variations in p, q and $D_{\mathrm{CaCO_3}}$.

For reference we first illustrate the simulation results for each standard set of parameters, obtained with a constant porosity $\phi \equiv \phi_0$. In the subsequent sections, we vary the relevant parameters and show the results for certain quantities for which the effects are particularly eminent.

5.1 Simulation of an accelerated carbonation test

In figures 2 and 3 we show the nondimensional concentration profiles of $CO_2(g)$, $CO_2(aq)$, $Ca(OH)_2$ (aq), moisture and $CaCO_3(aq)$ as well as the carbonation depth (see also section 3.4), the (bulk) carbonation degree, the reaction rate, and the reaction zone using the standard data set for the accelerated carbonation scenario, see appendix. All plots show dimensionless quantities. The length- and time-axis of the plots are drawn using dimensional quantities.

To compare the carbonation depth with experimental data we use the measurements by Papadakis *et al.*[6] (fig. 3a). A short description of the accelerated experimental setup can also be found there.

The nondimensionalisation allows the comparison of the magnitude or the *impact* of each term in the system of PDEs. We list the dimensionless parameters resulting from the standard data set in table 1. It can be seen that the parameters are of highly different magnitudes. For instance, Φ^2 is large, which means that the carbonation reaction is in its fast regime. The great magnitude of the interfacial-exchange numbers, W^{Hen}, W_1^{Rob}, and W_4^{Rob} imply a strong tendency to reach the respective equilibrium state. Note also that the value of δ_1, which accounts for the diffusion of $CO_2(g)$, is much greater than the other dimensionless diffusivities δ_ν, $\nu = 2, 3, 4, 5$.

β_1	β_2	β_3	β_4	β_5	Φ^2	W^{Hen}
1	0.848	196	540	196	993	750
δ_1	δ_2	δ_3	δ_4	δ_5	W_1^{Rob}	W_4^{Rob}
1	$8.33 \cdot 10^{-6}$	$8.33 \cdot 10^{-9}$	$8.33 \cdot 10^{-4}$	0	$2.50 \cdot 10^{4}$	$2.50 \cdot 10^{6}$

Table 1: Typical values of the nondimensional combinations for the accelerated setting

Cf. figures 2 and 3, we observe the formation of a reaction layer, near which fairly steep decays of the reactants ($CO_2(aq)$ and $Ca(OH)_2(aq)$) as well as $CO_2(g)$ are seen. The similarity of the profiles of $CO_2(g)$ and $CO_2(aq)$ hint at comparably small effects caused by the absorption terms in this setting, while the profiles of $CO_2(g)$ and moisture validate our choice of Robin constants to approximate Dirichlet boundary conditions at the exterior boundary of the sample.

[6] See figure 7a in [PVF89]. Here we are dealing with an OPC sample having the water-to-cement ratio $R_{w/c} = 0.50$ and the aggregate-to-cement ratio $R_{a/c} = 3$. The exposure conditions in the carbonation chamber are 50% CO_2(g), 65% RH, and 30°C.

From the moisture profiles we observe that the water produced by reaction leads to a drastic increase of moisture in the already carbonated part. This *water production layer* can lead to a noticeable decrease in the diffusion of $CO_2(g)$ if one accounts for this coupling which is not yet included in our model. This effect has been already observed by simulations in [IMS04]. See also section 5.4.

It can also be observed that although the reaction rate decreases with time, the width of the reaction layer remains fairly constant after a (short) *transient time*. This transient time is roughly the time required for the reaction layer to form and to begin moving. It can be read off the plot of the left boundary of the reaction zone (fig. 3d) as that point where the position of left boundary becomes greater than zero. With the current choice of parameters, the transient time is slightly less than a day. The transient time effects on such reaction-diffusion problems are not further investigated here.

5.2 Simulation of a natural carbonation test

In figures 4 and 5, we show the nondimensional concentration profiles of $CO_2(g)$, $CO_2(aq)$, $Ca(OH)_2$ (aq), moisture, and $CaCO_3(aq)$ as well as the carbonation depth, the carbonation degree, the reaction rate, and the reaction zone using the standard set of parameters for the natural carbonation scenario listed in the appendix (table 4).

The dimensionless parameters resulting from the standard data set of the natural setting are given in table 2. It can be seen that the ratios of the parameters are similar to those in the accelerated setting (cf. table 1). Only β_3, β_4 and β_5 are considerably greater due to the lower external $CO_2(g)$-concentration.

β_1	β_2	β_3	β_4	β_5	Φ^2	W^{Hen}
1	0.790	$2.91 \cdot 10^5$	$8.96 \cdot 10^5$	$2.91 \cdot 10^5$	$1.83 \cdot 10^3$	$2.81 \cdot 10^3$
δ_1	δ_2	δ_3	δ_4	δ_5	W_1^{Rob}	W_4^{Rob}
1	$6.25 \cdot 10^{-6}$	$6.25 \cdot 10^{-9}$	$6.25 \cdot 10^{-4}$	0	$1.88 \cdot 10^4$	$1.88 \cdot 10^6$

Table 2: Values of the nondimensional combinations for the standard natural setting

In figure 5a, we compare our results with measurements reported by Wierig in [Wie84]. His data refers to a CEM I concrete sample with $R_{w/c} = 0.60$ placed out of doors under roof.[7]

We generally observe a similar behaviour of the profiles as for the accelerated case, but over a different time span. The only profile which is highly different is that of moisture (cf fig. 2c vs. fig. 4c). Here we observe lower profiles as in the accelerated case. This gives rise to the assumption that in the natural carbonation setting, the water produced by carbonation is less significant. In other words, whilst the accelerated test leaves the carbonated sample relatively wet, the test under natural exposure conditions offers enough time to the concrete to dry out. Note also that for this choice of parameters, the transient time is roughly one year.

[7] See table 2, sheet 1 and a description of the experimental setup in [Wie84]. The natural carbonation test was carried out in Zement- und Betonlaboratorium, Beckum, Germany. The local climatic conditions take the average annual values of 78% RH and 9°C.

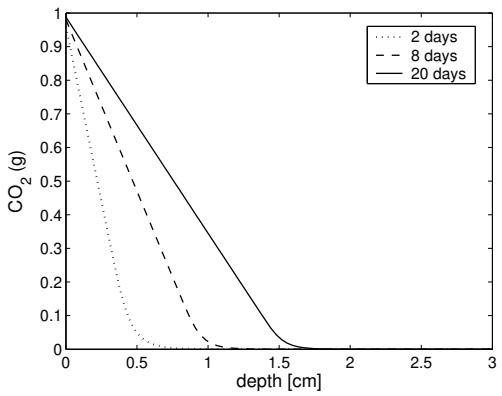

a) $CO_2(g)$

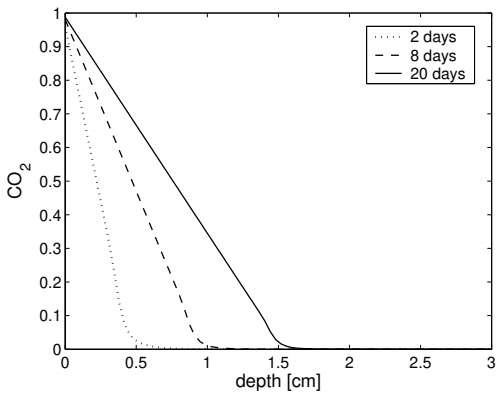

b) $CO_2(aq)$

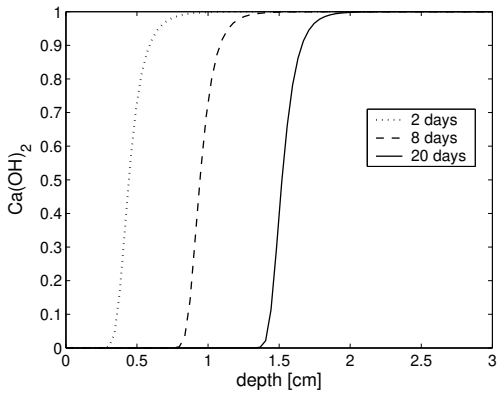

c) $Ca(OH)_2(aq)$

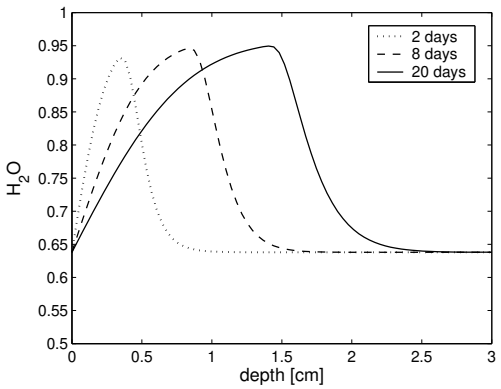

d) moisture

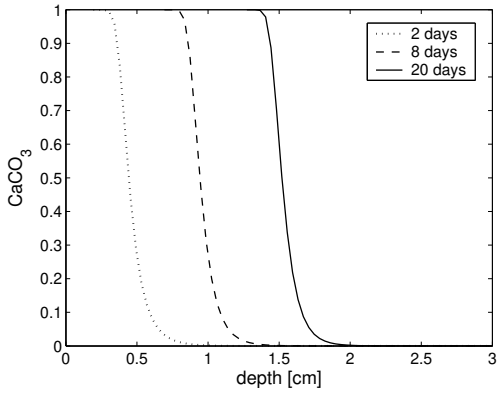

e) $CaCO_3(aq)$

Figure 2: Concentration profiles of the involved species obtained with the standard set of parameters in the accelerated scenario (cf. appendix).

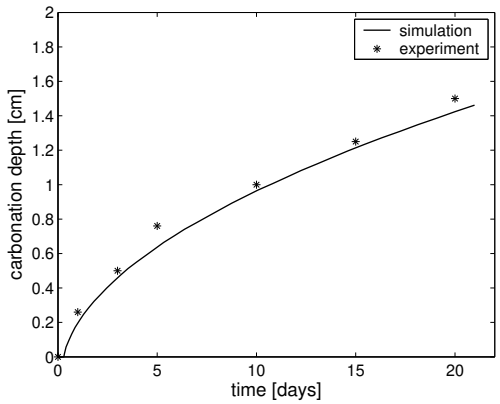

a) carbonation depth

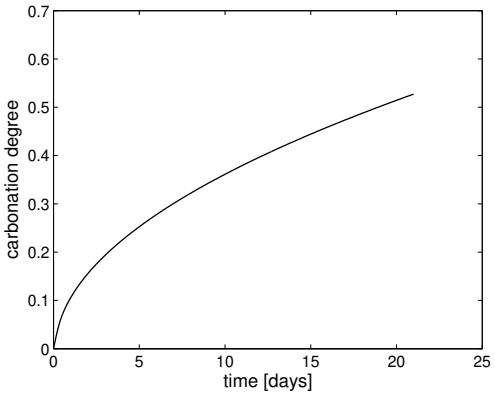

b) carbonation degree

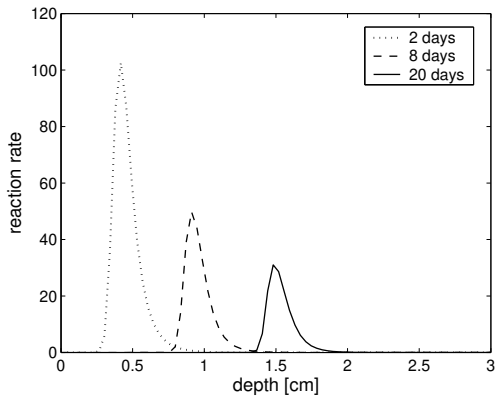

c) reaction rate

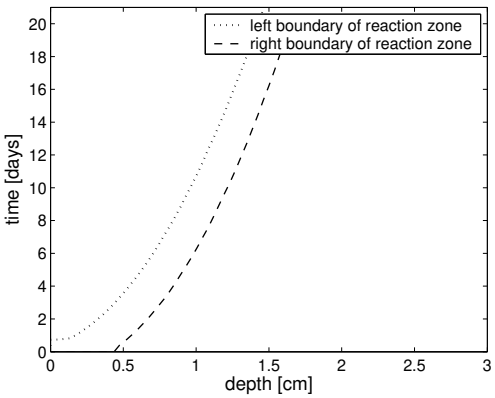

d) reaction zone

Figure 3: Profiles of carbonation depth, carbonation degree, reaction rate, and reaction zone obtained with the standard set of parameters in the accelerated scenario (cf. appendix).

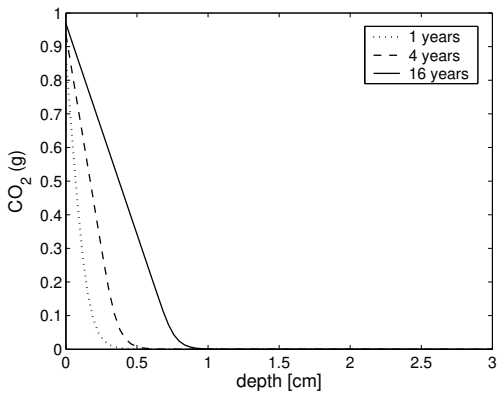

a) $CO_2(g)$

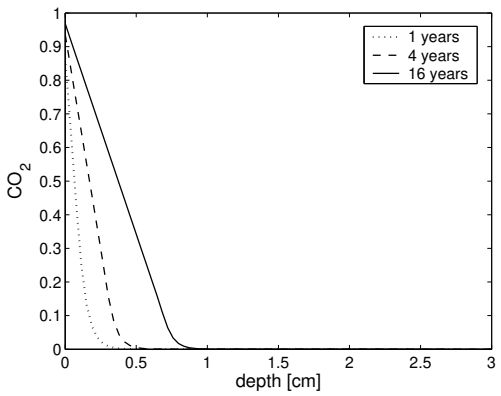

b) $CO_2(aq)$

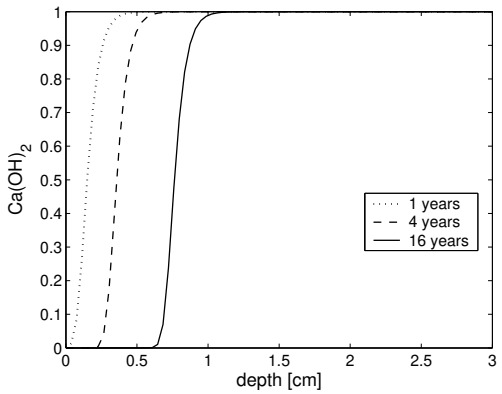

c) $Ca(OH)_2(aq)$

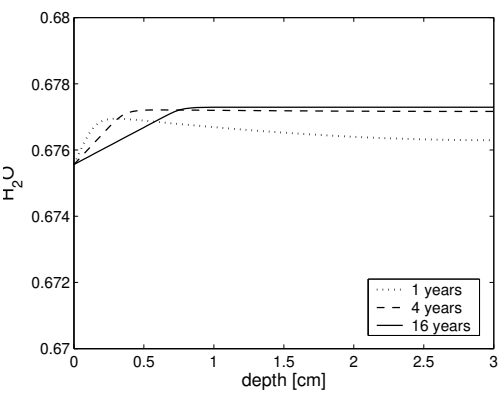

d) moisture

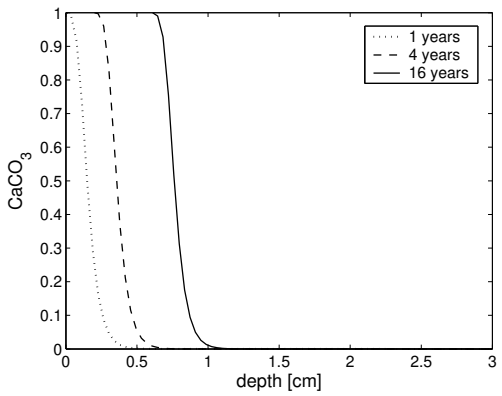

e) $CaCO_3(aq)$

Figure 4: Concentration profiles of the involved species obtained with the standard set of parameters in the natural carbonation scenario (cf. appendix).

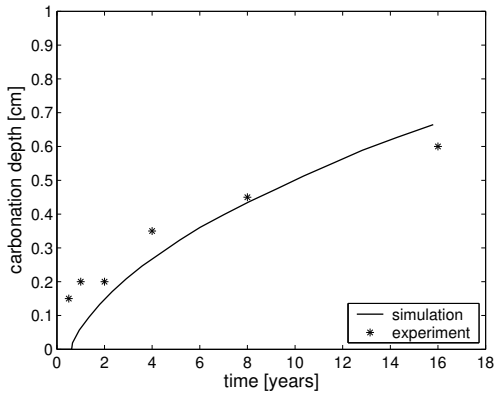

a) carbonation depth

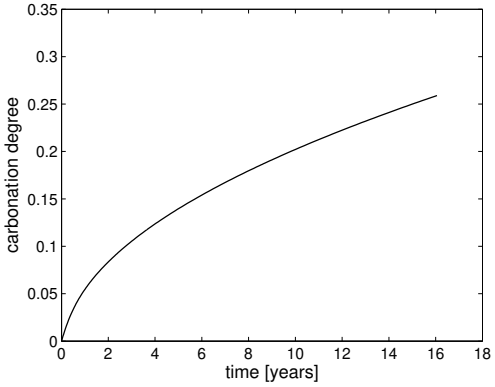

b) carbonation degree

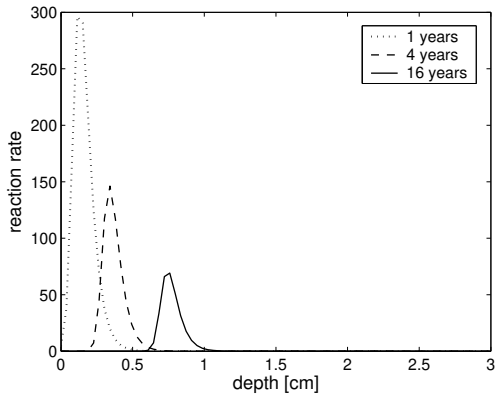

c) reaction rate

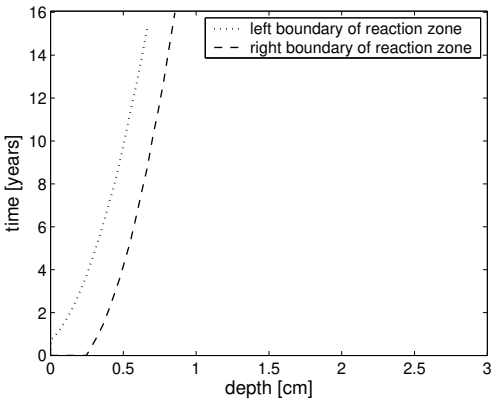

d) reaction zone

Figure 5: Profiles of carbonation depth, carbonation degree, reaction rate, and reaction zone obtained with the standard set of parameters in the natural carbonation scenario (cf. appendix).

5.3 Effects due to the variation of model parameters

In this subsection, we discuss the influence of some relevant parameters on the penetration curves, i.e. the Thiele modulus as well as the mass transfer coefficients of the gas absorption at the gas-liquid interface and at the outer boundary. We use the accelerated carbonation data for this illustration.

5.3.1 Thiele modulus

The most important dimensionless combination in our model is the Thiele modulus Φ^2. It relates the rapidness of the carbonation reaction to the diffusion time of $CO_2(g)$ and is given by

$$\Phi^2 = \frac{L^2 m_{CO_2} (c_2^m)^p (c_3^m)^q}{D_{CO_2(g)} c_1^m} C^{reac}. \tag{5.2}$$

As discussed previously, for the carbonation scenario we are in the fast-reaction regime, i.e. $\Phi^2 \gg 1$. We illustrate the effects caused by a Thiele modulus differing from that of the standard setting ($\Phi^2 \approx 10^3$) by a factor of 10, namely $\Phi_1^2 \approx 10^2$ and $\Phi_2^2 \approx 10^4$. Note that a variation of Φ^2, while leaving all other parameters unchanged, can also be interpreted as the same variation in the reaction constant C^{reac}.

We begin by describing the effect of a smaller Thiele modulus. If Φ_1^2 is chosen instead of Φ^2 and all other parameters are left unchanged, it can be seen that the advancement of the carbonation front is much slower (cf. fig. 6a vs. fig. 3a). The maximum of the reaction rate is much smaller at all times (cf. fig. 6c vs. fig. 3c), the width of the reaction zone is greater (cf. fig. 6d vs. fig. 3d), but the carbonation degree remains almost unchanged (cf. fig. 6b vs. fig. 3b). It is only slightly smaller compared to the standard setting. Note that the transient time is almost five times as long. For all species, it can be said that the concentration profiles are not as sharp but seem smoother than those obtained with the standard set of parameters.

If Φ_2^2 is chosen instead of Φ^2 and all other parameters are left unchanged, it can be seen that the advancement of the carbonation front is a bit faster (cf. fig. 7a vs. fig. 3a), the maximum of the reaction rate is much larger at any given time (cf. fig. 7c vs. fig. 3c), the width of the reaction zone is smaller (cf. fig. 7d vs. fig. 3d) but the carbonation degree remains almost unchanged again (cf. fig. 7b vs. fig. 3b). It is only slightly larger compared to the standard setting. The transient time is negligible in this setting, i.e. the reaction layer is formed and begins moving almost instantaneously. The concentration profiles of all species have somewhat sharper decays than those obtained with the parameters of the standard setting. A noticeable spreading or sharpening of the layer does *not* occur. Moreover, note that the experimental data is slightly better approximated. Furthermore, it can be observed that only relatively small changes are found if the Thiele number is chosen even larger (e.g. $\Phi_3^2 = 1000 \cdot \Phi^2$), i.e. a kind of formal convergence to a certain configuration is observed for very large Thiele numbers.

Remark 5.1 *It should be noted that in the* moving-interface carbonation models *introduced in [BKM03a, BKM03b] the width ϵ of the rection layer is proportional to $\frac{1}{\Phi^2}$. This result is essentially based on the use of an* a priori *given dynamic law to move the layer. See details in [Mun05]. Note that the proportionality $\epsilon \sim \frac{1}{\Phi^2}$ is only a rough scaling. Asymptotically, one can derive a precise scaling of the reaction front accounting for the nonlinearities in the carbonation kinetics. Compare [BS00] and [Do82] for some studies in this direction.*

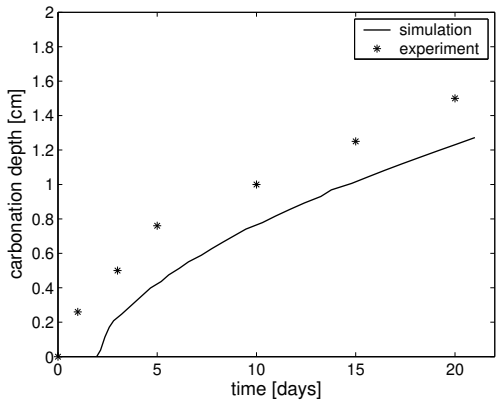

a) carbonation depth, $\Phi_1^2 \approx 10^2$

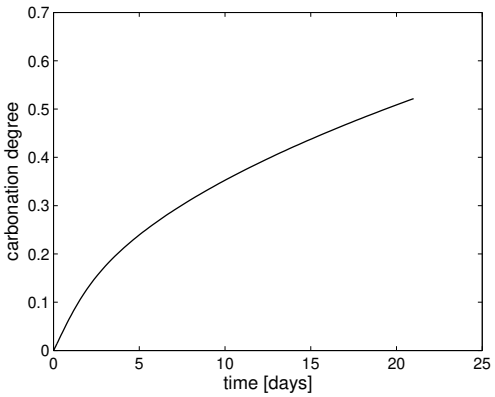

b) carbonation degree, $\Phi_1^2 \approx 10^2$

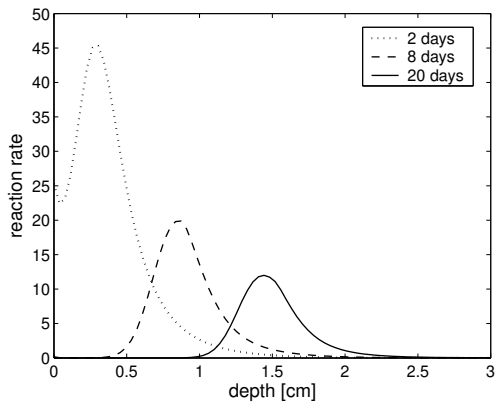

c) reaction rate, $\Phi_1^2 \approx 10^2$

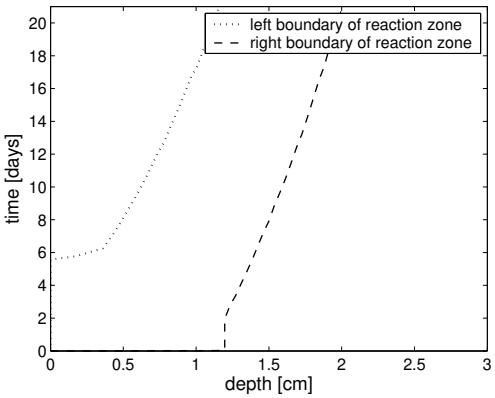

d) reaction zone, $\Phi_1^2 \approx 10^2$

Figure 6: Profiles of carbonation depth, carbonation degree, reaction rate, and reaction zone obtained with $\Phi_1^2 = 0.1 \cdot \Phi^2 \approx 10^2$.

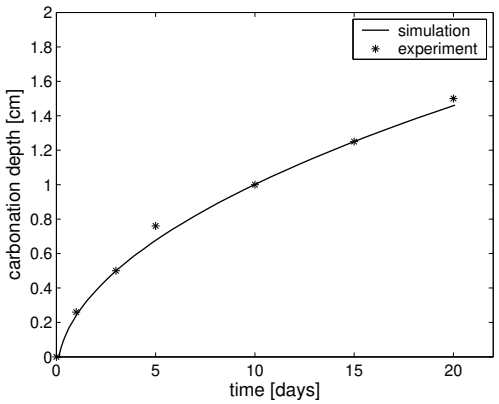

a) carbonation depth, $\Phi_2^2 \approx 10^4$

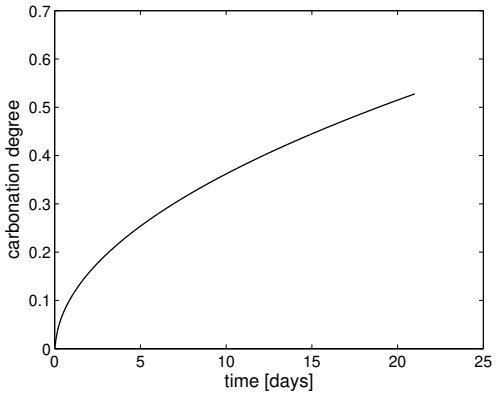

b) carbonation degree, $\Phi_2^2 \approx 10^4$

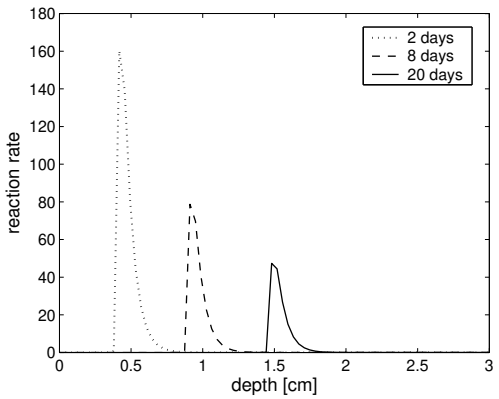

c) reaction rate, $\Phi_2^2 \approx 10^4$

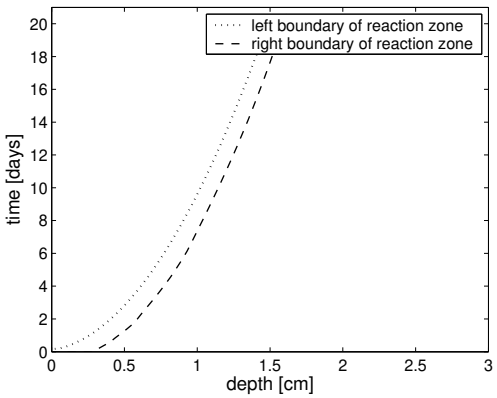

d) reaction zone, $\Phi_2^2 \approx 10^4$

Figure 7: Profiles of carbonation depth, carbonation degree, reaction rate, and reaction zone obtained with $\Phi_2^2 = 10 \cdot \Phi^2 \approx 10^4$.

5.3.2 CO_2-absorption coefficient

We want to emphasise in which way our results are influenced by the way the absorption of CO_2 in water is modelled. With the standard linear ansatz based on Henry's law and one-film theory (cf. (3.6)), there is exactly *one* parameter accounting for the local geometry and for the approximate time scale of absorption, namely the mass transfer coefficient C^{ex}. The exact size of this constant is generally *unknown* for concrete-based materials. It enters into the nondimensional number

$$W^{\mathrm{Hen}} = \frac{L^2}{D_1} C^{\mathrm{ex}}. \tag{5.3}$$

This can be interpreted as the ratio between the *characteristic diffusion time* and the *characteristic time of interfacial mass transfer*. For a large value of this constant, absorption is controlled by diffusion of $CO_2(g)$, and the equilibrium of the CO_2 concentrations in water and gas is achieved in almost the whole volume Ω. In this case, we expect our results to be unsensitive on the exact choice of the parameter C^{ex}. If we choose W^{Hen} small, diffusion (and, consequently, reaction) become more influenced by CO_2-transfer at the air-water interface which leads to a complication of the system. In general, only the first behaviour is assumed to happen in the carbonation scenario.

For the parameter setting based on accelerated conditions (cf. table 4 in the appendix), CO_2-absorption is relatively large ($W^{\mathrm{Hen}} = 750$). We compare the results with other regimes of W^{Hen} by varying C^{ex} and leaving all other parameters as constant. The following effects can be observed:

- For values of W^{Hen} *larger* than 750, all concentration profiles remain nearly unchanged.
- For values of W^{Hen} *smaller* than 750 ($W^{\mathrm{Hen}} = 75$ and 37.5), the effects can be summarized as follows
  1. The profile of $CO_2(aq)$ exhibits a steeper gradient near the reaction front (fig. 8b,d,f).
  2. $CO_2(g)$ penetrates deeper into the concrete (fig. 8a,c,e).
  3. The reaction zone is wider (fig. 9a).
  4. The maximum value of the reaction rate is lower (fig. 9b).
  5. The carbonation front takes longer time to form, but propagates analogously (fig. 10b). Consequently, the carbonation degree at any given time is smaller (fig. 10a).

The same trend in propagation of the front – after a transient time during which it is formed – can be explained by the observation that two effects are compensating: At a given point within the reaction zone, less $Ca(OH)_2$ is reacting, but on the other hand, the reaction zone is wider due to the deeper penetration of CO_2.

We may conclude that in our model a slow absorption of CO_2 in water leads to a broadening of the reaction front and a longer transient time. For large times, the total consumption of $Ca(OH)_2$ (and thus, the carbonation depth) do not change very much.

5.3.3 External exchange coefficient for CO_2

To investigate the influence of the boundary conditions for CO_2, we make similar numerical experiments as in the preceding sections. The exchange of CO_2 with the environment is described by the dimensionless parameter C^{Rob}. The corresponding dimensionless number is

$$W_1^{\mathrm{Rob}} = \frac{L}{D_1} C_1^{\mathrm{Rob}}. \tag{5.4}$$

This represents the ratio between the *characteristic diffusion time* and the *characteristic time of interfacial mass transfer* at the exposed boundary. For large values of this number, the interfacial mass transfer is fast compared to diffusion. In this case, we expect the CO_2-concentration to

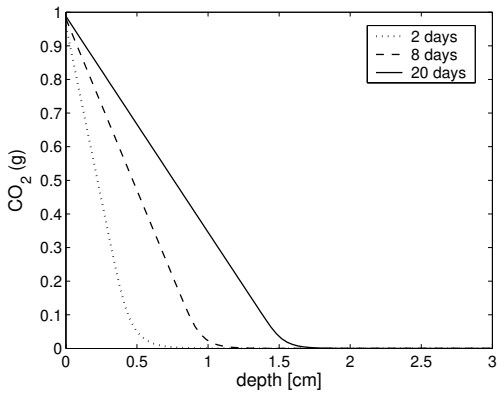

a) $CO_2(g)$, $W^{\mathrm{Hen}} = 750$

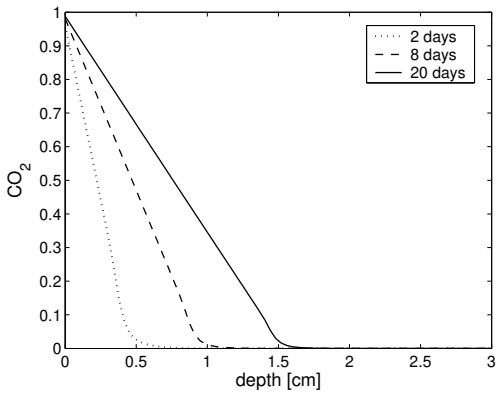

b) $CO_2(aq)$, $W^{\mathrm{Hen}} = 750$

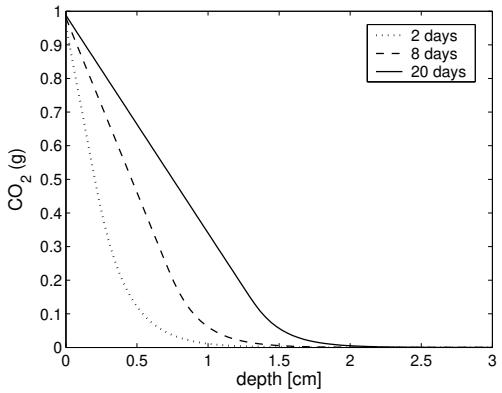

c) $CO_2(g)$, $W^{\mathrm{Hen}} = 75$

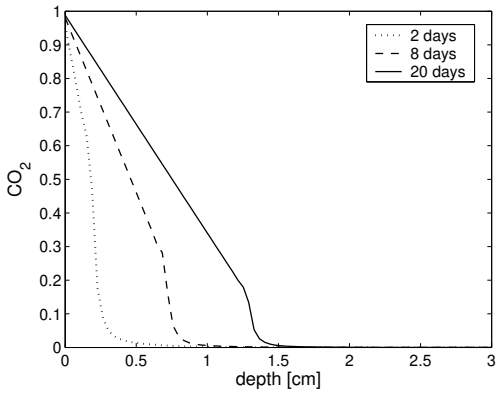

d) $CO_2(aq)$, $W^{\mathrm{Hen}} = 75$

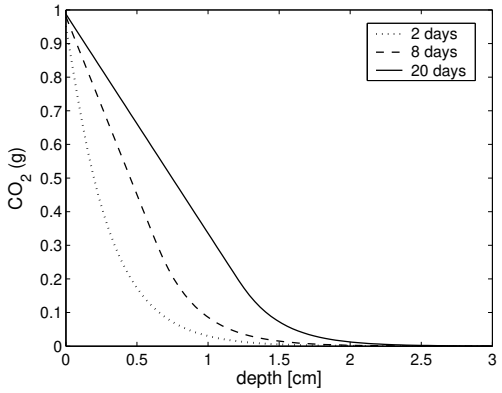

e) $CO_2(g)$, $W^{\mathrm{Hen}} = 37.5$

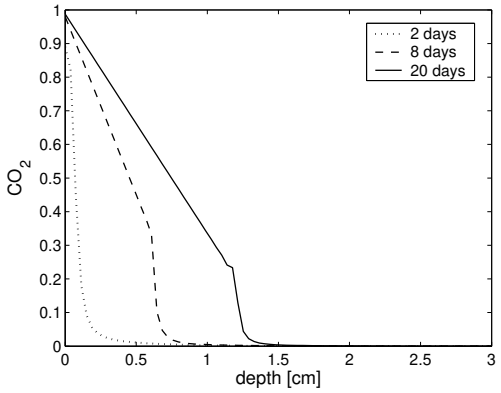

f) $CO_2(aq)$, $W^{\mathrm{Hen}} = 37.5$

Figure 8: CO_2-profiles in air and pore water for different values of W^{Hen}. a+b) Fast absorption. c+d) Moderatly fast absorption. e+f) Slow absorption.

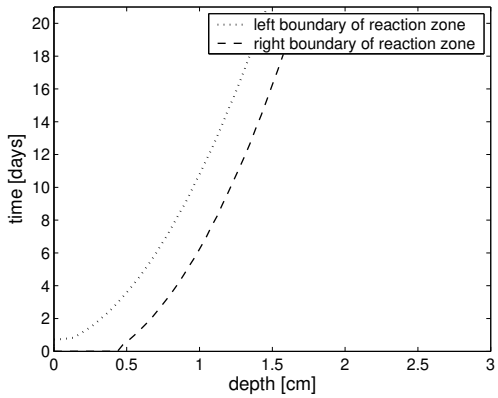

a) reaction zone, $W^{\mathrm{Hen}} = 750$

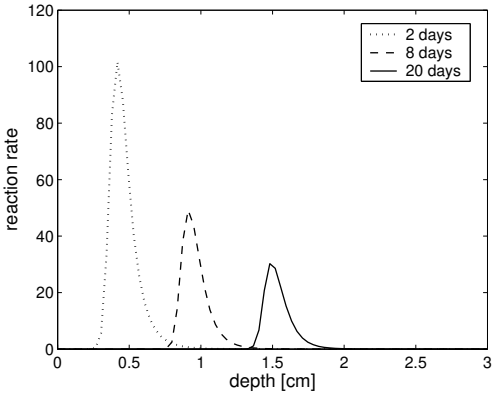

b) reaction rate, $W^{\mathrm{Hen}} = 750$

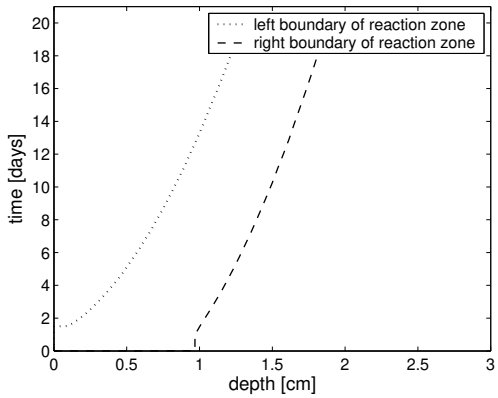

c) reaction zone, $W^{\mathrm{Hen}} = 75$

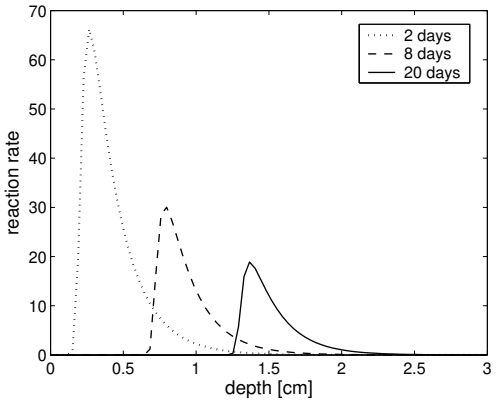

d) reaction rate, $W^{\mathrm{Hen}} = 75$

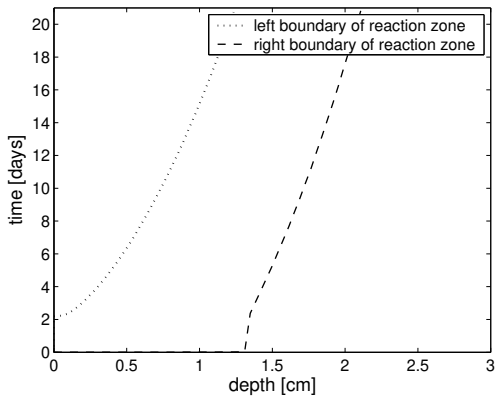

e) reaction zone, $W^{\mathrm{Hen}} = 37.5$

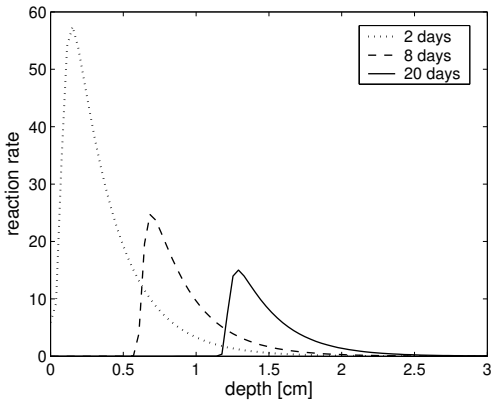

f) reaction rate, $W^{\mathrm{Hen}} = 37.5$

Figure 9: Reaction zone and reaction rate for different values of W^{Hen}. a+b) Fast absorption. c+d) Moderatly fast absorption. e+f) Slow absorption.

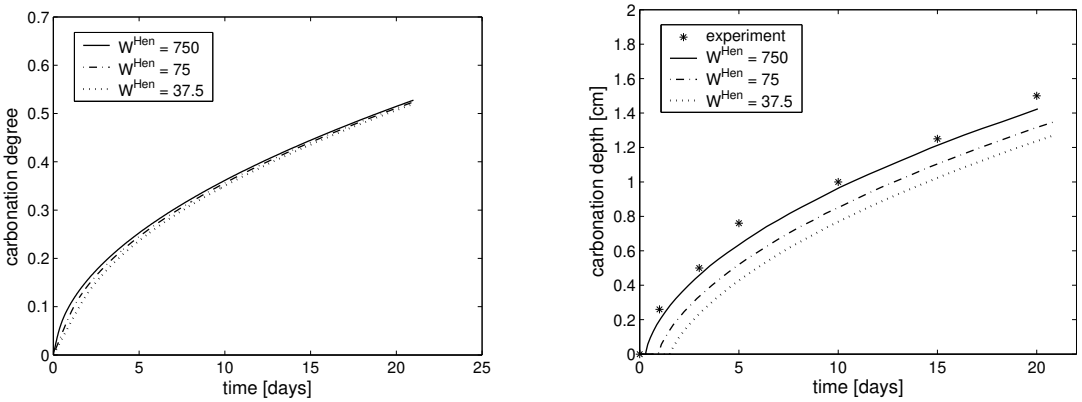

a) Carbonation degree b) Carbonation depth

Figure 10: Carbonation degree and carbonation depth for $W^{\mathrm{Hen}} = 750, 75, 37.5$. For a slower absorption, carbonation is also slower due a larger transient time. For large time, all profiles exhibit the same behaviour.

nearly equal the ambient concentration. In other words, we expect that the $CO_2(g)$-profile formally converges to a profile corresponding to Dirichlet conditions. We therefore refer to this case as the *quasi-Dirichlet*-case. For a small value of W_1^{Rob}, the interfacial mass transfer is slow. We then expect a more complicated behaviour of the carbonation process with a strong dependence on the exact value of W_1^{Rob}.

We choose the standard parameter setting based on accelerated conditions, with a fast interfacial exchange ($W_1^{\mathrm{Rob}} = 25000$). Varying the constant C_1^{Rob} (and implicitly W_1^{Rob}) we observe the following:

- For values of W_1^{Rob} *larger* than 25000, the profiles remain almost the same.
- For values of W_1^{Rob} *smaller* than 25000 ($W_1^{\mathrm{Rob}} = 2500, 250$), we observe the following:
  1. The $CO_2(g)$ concentration at the outer boundary as well as the penetration depth are much *lower* than in the quasi-Dirichlet-case (fig. 11). The same happens with the $CO_2(aq)$-profiles (not shown here).
  2. The carbonation front is formed later. It deviates from a $\sqrt{t}$-behaviour to an almost linear dependence on t (fig. 12b), at least near the exposed boundary. The carbonation degree at a given time is lower (fig. 12a).

As a conclusion, we note that the *resistance* to CO_2 at the outer boundary can play a significant role for carbonation. However, according to experimental data, the mass-transfer coefficient for CO_2 seems to be sufficiently large such that Dirichlet conditions can also be used.

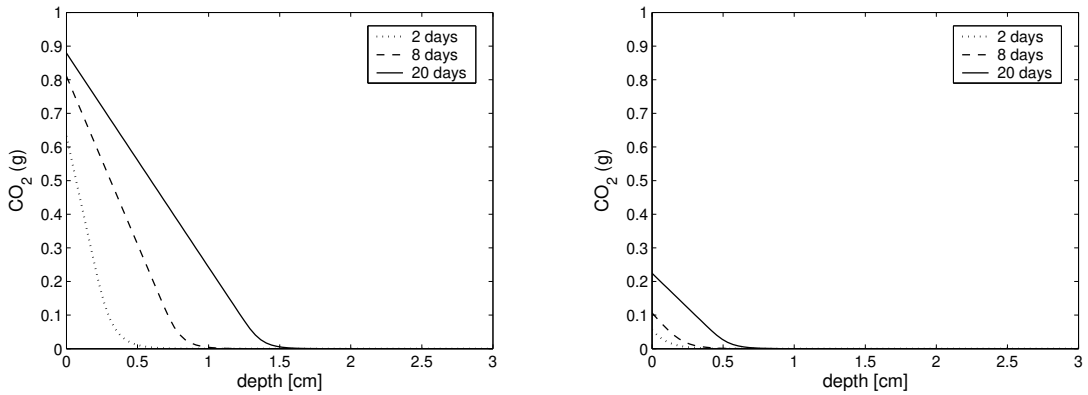

a) $CO_2(g)$, $W_1^{\mathrm{Rob}} = 2500$ b) $CO_2(g)$, $W_1^{\mathrm{Rob}} = 250$

Figure 11: $CO_2(g)$-profiles for different values of W_1^{Rob}. a) Fast interfacial mass transfer; the concentration of $CO_2(g)$ on the boundary almost coincides with the ambient value. b) Slow interfacial mass transfer.

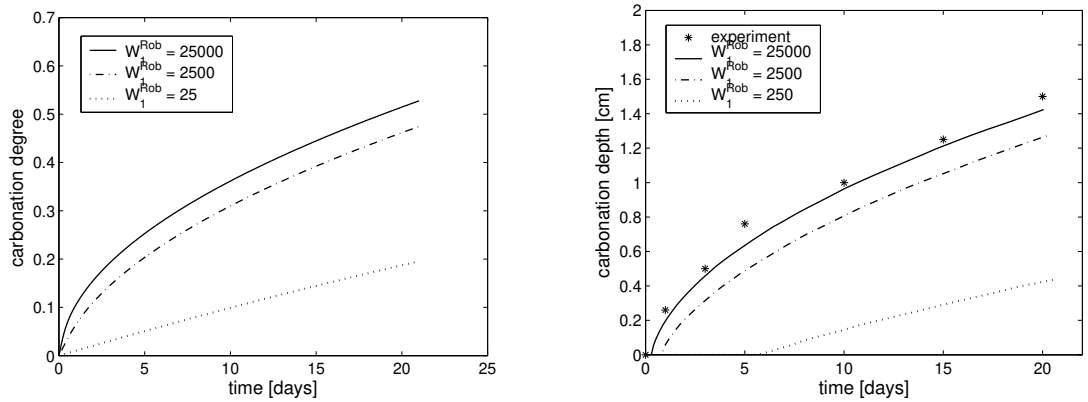

a) carbonation degree b) carbonation depth

Figure 12: Carbonation degree and carbonation depth for $W_1^{\mathrm{Rob}} = 25000$, 2500, 250.

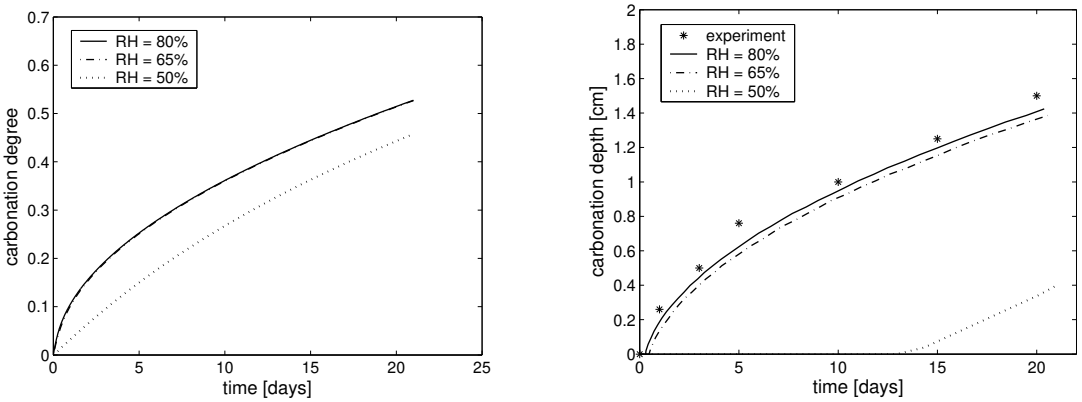

a) carbonation degree b) carbonation depth

Figure 13: Carbonation degrees and carbonation depth for constant values RH $\approx 50\%$ as well as RH $= 65\%$ and 80%

5.4 Effect of moisture

In our model, the moisture enters in the carbonation process through the factor f^{hum} in the carbonation-reaction rate (cf. (3.3)). By making use of numerical experiments, we would like to give answers to the following questions concerning our model:

1. What is the effect of a given constant moisture (RH $\in [50\%, 80\%]$) on the carbonation process when neglecting the coupling by water production?
2. What are the differences between the setting in 1. and the fully coupled model? How does the model depend on the additional parameters, i.e. on the diffusivity and interfacial mass transfer coefficient of moisture?
3. What is the effect of a time-dependent, particularly of a periodic, ambient humidity? Which different effects are obtained by imposing such a profile *directly* in the equations, or (in a coupled system) at the boundary?
4. How important is the production of water by carbonation for the whole setting?

Regarding the last question, we have already observed the occurrence of a *water- production layer* in case of the accelerated setting (cf. section 5.1). Further aspects will be pointed out in the following three subsections.

5.4.1 Moisture as a given constant

In figure 13, carbonation degrees and depths for different (constant) values of relative humidity between 50% and 80% are shown in the accelerated carbonation regime. The coupling terms are neglected here. A constant moisture is directly plugged into the carbonation reaction rate. Due to the monotonic increasing humidity factor in the reaction rate, we observe a *stronger* reaction in case of a *higher* moisture content and therefore a slightly *higher* penetration depth. For RH $\searrow 50\%$, carbonation becomes very low because, cf. (3.4), the reaction rate vanishes in this case. For RH $> 65\%$, the profiles do almost not change with altering RH.

5.4.2 Moisture as a solution of a PDE

Now we compare the results from the decoupled setting with those from the *fully coupled* model. Here, the same values for relative humidity are imposed at the exposed boundary ($\mathrm{RH}^{\mathrm{ext}} \approx 50\%$ as

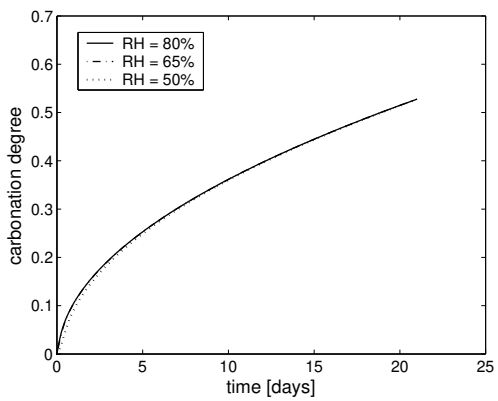

a) carbonation degree

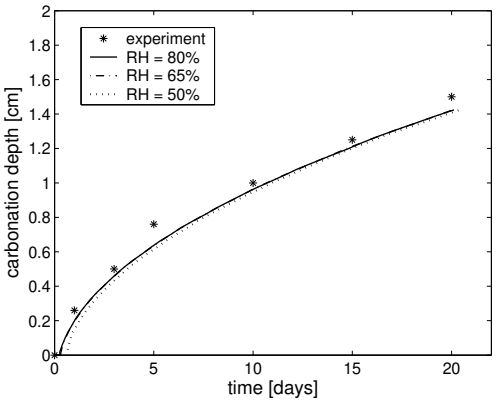

b) carbonation depth

Figure 14: Carbonation degrees and carbonation depth for RH $\approx 50\%$ as well as RH $= 65\%$ and 80%, prescribed at the outer boundary

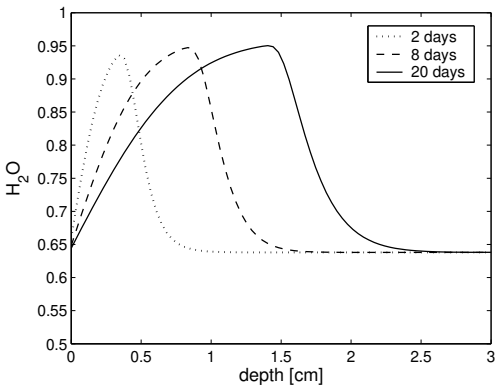

a) moisture $W_4^{\mathrm{Rob}} = 25$

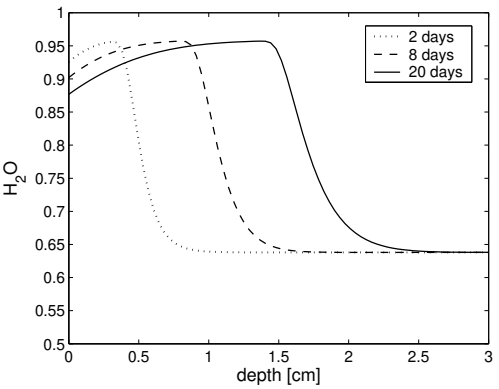

b) moisture, $W_4^{\mathrm{Rob}} = 0.25$

Figure 15: Total water concentration for different values of W_4^{Rob}. a) Fast mass transfer at the exposed boundary (quasi-Dirichlet-case). b) Slow mass transfer.

well as RH $= 65\%$ and 80%). With the transport parameters for moisture chosen in the appendix and a *high* ambient humidity we obtain almost the same curves for carbonation degree and depth as for the decoupled setting, cf. figure 14. In contrast, for a *low* humidity ($\mathrm{RH}^{\mathrm{ext}} \approx 50\%$) we obtain higher profiles as in the decoupled setting. We assume that this is an effect of the water produced by carbonation.

Additionally, we vary the value of the exchange coefficient at the boundary, $C_{\mathrm{H_2O}}^{\mathrm{Rob}}$ and, accordingly, the value of the dimensionless number W_4^{Rob} (cf. the discussion in section 5.3.3). The right choice of boundary conditions seems to be of much more importance than for CO_2, as it is not quite clear whether the mass transfer can be considered as being sufficiently fast (cf. section 2.3). We observe a higher water content for smaller values of W_4^{Rob} near the exposed boundary (fig. 15). In this special case of *not time-dependent* boundary conditions, an effect on carbonation is almost not noticeable.

We expect stronger effects if we account for the lower transport of CO_2 due to increased moisture. Therefore, a more sophisticated model for the coupling of water with transport of the other substances is needed.

5.4.3 Effects of periodic moisture inputs

We are interested to see how our model behaves in case of a natural carbonation scenario. Therefore, we suppose an ambient humidity that depends on seasonal effects. Steffens [Ste00] proposes a relative humidity range between 71% in May and 86% in December for the northwestern part of Germany. We use this RH range for our boundary conditions. Other climatic effects like change in temperature or rainfall are neglected.

We compare three different modelling scenarios:

1. A PDE for moisture with time-dependent boundary conditions and *fast exchange* at the boundary (quasi-Dirichlet-case).
2. A PDE for moisture with time-dependent boundary conditions and *slow exchange* at the boundary.
3. An *a priori* given periodic moisture profile.

The results are shown in figure 16. For a faster moisture transfer at the boundary (fig. 16a), we observe a larger value at the boundary, but a slightly lower profile far away from it. This can be explained by a stronger *drying effect* during the months when the ambient humidity is low. The influence on the zone where the carbonation reaction takes place can be seen in (fig. 16c and d). The curves exhibit some small oscillations, in particular in the first three years. This effect is naturally weaker in the case of a slow exchange at the boundary.

However, at least with this choice of parameters, the differences in the moisture profiles seem to be too small to have noticeable effects on the carbonation depth, see (fig. 16e and f). Again we expect further effects with an improved model, for instance a decrease in the carbonation speed during months of high humidity.

Remark 5.2 *It can also be interesting to investigate the effects of inputs as a superposition of two or more period lengths. For example, one could choose a period length of one year, and a second one of one day. Within such a modelling frame one could account, for instance, for daily fluctuations in humidity and temperature, or tidal effects, in the case of marine structures exposed to sea water.*

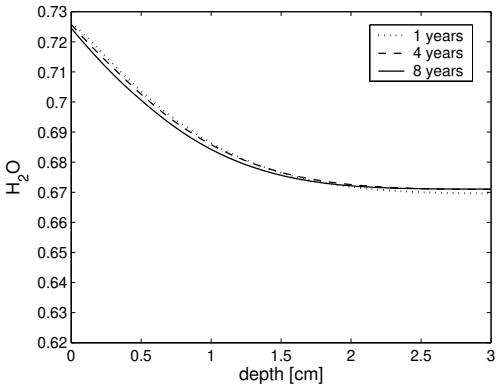

a) moisture, $W_4^{\mathrm{Rob}} = 19$

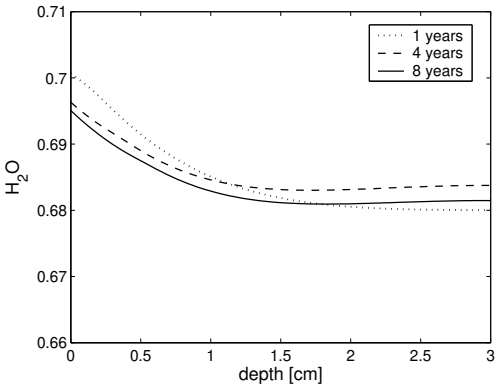

b) moisture, $W_4^{\mathrm{Rob}} = 0.19$

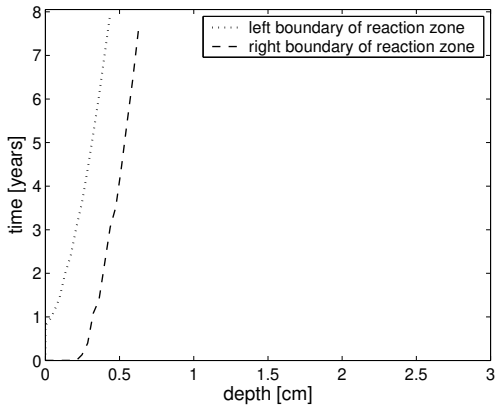

c) reaction zone, $W_4^{\mathrm{Rob}} = 19$

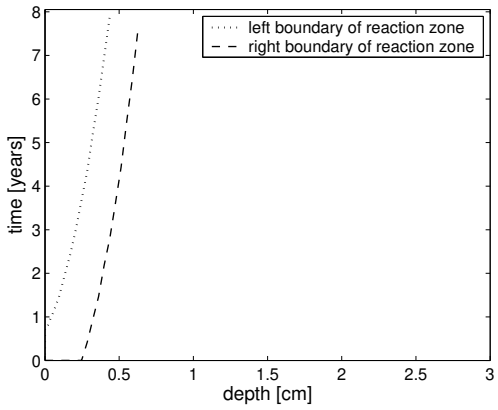

d) reaction zone, $W_4^{\mathrm{Rob}} = 0.19$

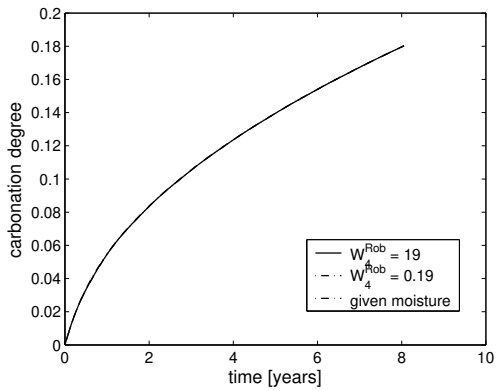

e) carbonation degree

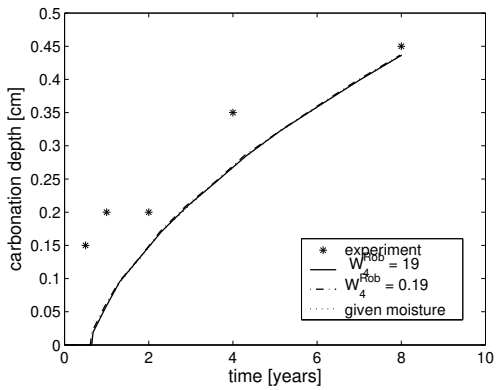

f) carbonation depth

Figure 16: Moisture profiles and carbonation progress for different periodic input scenarios. a, b) Moisture profiles for fast (a) and slow (b) exchange at the boundary. c, d) Reaction zone for fast (a) and slow (b) exchange at the boundary. e, f) Carbonation degree and depth for the above two cases and for a given (i.e. decoupled) moisture profile.

5.5 Effects of time-dependent porosity

As discussed in section 2.1, we are also interested in what happens if the porosity of the concrete sample changes with time, i.e. it becomes smaller due to the conversion of $Ca(OH)_2$ into $CaCO_3$. In order to avoid additional effects motivated by the production of water we only consider this influence in the natural carbonation setting. As proposed in section 2.1 (cf. (2.2)) we use an exponential law for the evolution of the (space-independent) porosity $\phi(t)$. This yields an evolution of porosity illustrated in figure 17, i.e. the porosity has decreased by about one third of the initial value by the end of our considerations (after 16 years).

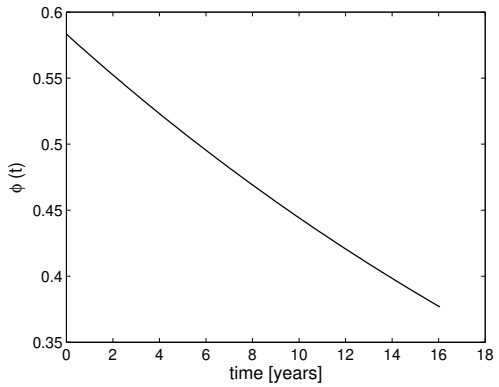

Figure 17: Evolution of the porosity $\phi(t)$. Here $\alpha = -4.19 \cdot 10^{-5}$ (cf. (2.2)).

The results for this choice of $\phi(t)$ are illustrated in figure 18. Compared to the setting with constant porosity (fig. 5) no changes are observed for small times which is not surprising as the initial porosity $\phi(0)$ coincides with the constant value from the standard setting. However, for larger times, it can be seen that the velocity of the reaction layer becomes smaller (fig. 18a) and its width decreases (fig. 18d). This yields a smaller carbonation degree (fig. 18b vs. fig. 5b) after 16 years.

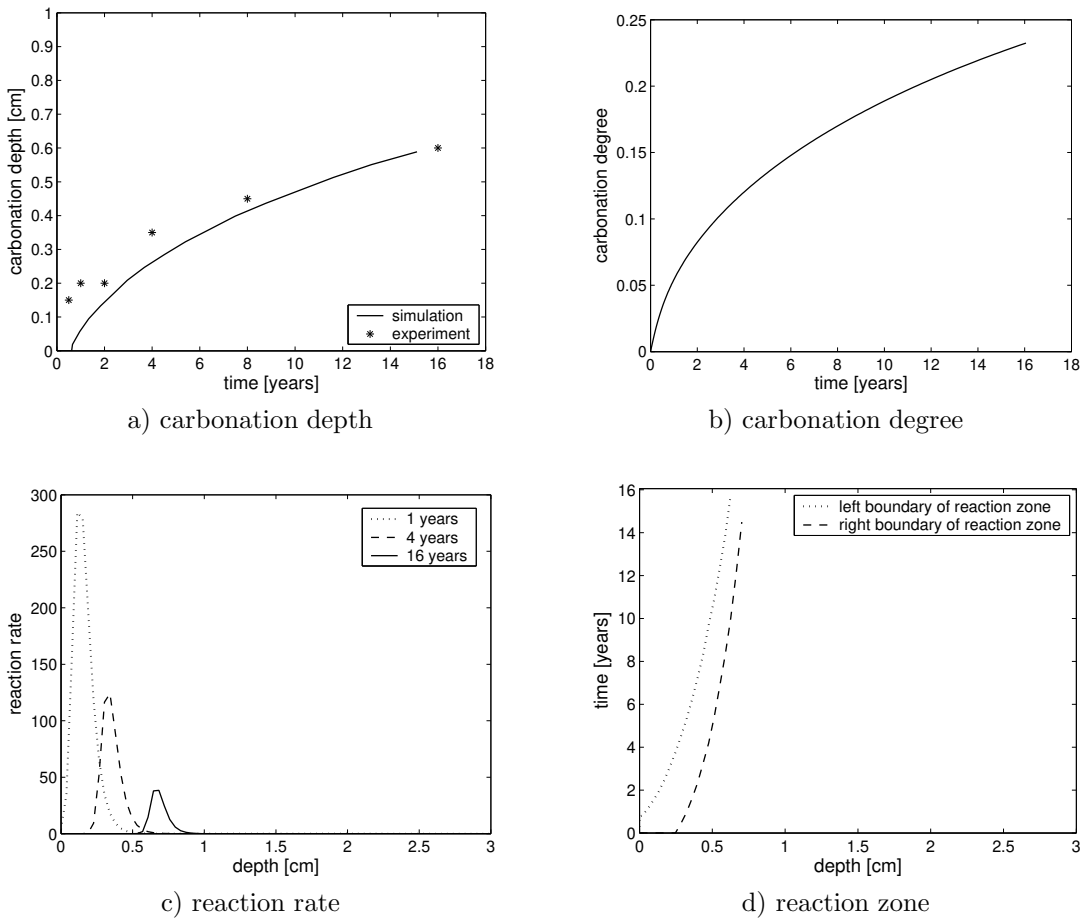

a) carbonation depth

b) carbonation degree

c) reaction rate

d) reaction zone

Figure 18: Profiles of carbonation depth, carbonation degree, reaction rate, and reaction zone obtained with time-dependent porosity as in figure 17 and parameters from the natural carbonation scenario.

6 Summary and Discussion

In both the accelerated and the natural scenario, the model is capable to predict the measured carbonation depths. Thereby, the localisation of the carbonation reaction on a thin layer can be observed for a wide range of parameters. This layer can be seen as a zone where a noticeable reaction takes place and near which steep gradients in the reactant profiles occur. The *width of the reaction layer* strongly depends on the Thiele modulus Φ^2. It is also related to the magnitude of the CO_2 absorption speed, which is quantified here by W^{Hen}. Roughly it can be said that the layer width increases if W^{Hen} or Φ^2 decreases. A noticeable spreading or sharpening with time does not occur, as long as the porosity can be assumed constant. The *speed of the layer* shows an opposite dependence, with a tendency to converge to a certain limit for large Thiele moduli. It seems to be less affected by the time scale of CO_2 absorption. Additionally, a transient time needed for the formation of the layer can be noticed.

The *production of water* by carbonation can lead to a drastic change in the moisture distribution, especially under *accelerated testing conditions*. In this case we observe much higher moisture profiles in the carbonated part of the concrete which can form a *water barrier* for the diffusing CO_2. However, if the Thiele modulus is large, the influence of water on the carbonation process via the humidity factor $f^{\mathrm{hum}}(w)$ (cf. (3.3)) is only of relevance for low humidity (50–60% RH). We expect stronger effects as soon as an improved coupling of the moisture with the CO_2 transport is incorporated in the model. A coupling of this kind can be obtained, for instance, by a model where the water fraction ϕ^{w} is dynamically related to the moisture variable w. For such a model, we also expect a larger influence of the boundary conditions for water on the carbonation process. With the model and the parameters considered here, a variation in the exchange coefficient as well as periodic ambient humidities lead to strong changes in the moisture profiles. Nevertheless, only small changes occur in the penetration depths. The periodic inputs can become particularly important if the mass transfer of water at the exposed boundary is sufficiently fast.

The different moisture profiles obtained under *accelerated conditions* and in the *natural carbonation setting* indicate that both cases can *not be treated analogously*. This topic is of special interest when accelerated experiments are designed to predict a life-time scenario.

We also observed that a *decrease in porosity*, imposed on our model, leads to a decrease of the speed and the width of the reaction layer for large times. Consequently, the whole carbonation process slows down for large times as it happens in reality.

The computation time basically depends on the size of the Thiele modulus. For large values, the system of first order ODEs in time, obtained after a semi-discretisation in space, is highly stiff. This requires the choice of very small time steps. Using an adaptive implicit method, it can be solved in a satisfactory way. Another numerical problem originating from a high Thiele modulus is the occurrence of (naturally) steep gradients of the concentration profiles near the internal layer. In order to catch effects in this zone, a sufficiently high resolution in space is needed. This issue is particularly eminent for an implementation in 2D or 3D for complex geometries. Adaptive discretisation methods are likely to solve this problem. For a first approach in this direction, we refer to [SMB05].

Acknowledgements

This work has been partially supported by the Deutsche Forschungsgemeinschaft (DFG) with a grant through the special priority program SPP1122 *Prediction of the Course of Physicochemical Damage Processes Involving Mineral Materials*. We also thank J. Grunewald, J. Kropp, K. Sisomphon and L. Franke for fruitful discussions.

Appendix: Dimensional parameters

We list the *standard* sets of dimensional parameters of the reference setting which we use for the numerical simulations. There are some parameters which are definite, for instance the molecular weights of the involved species. Others are generally unknown, for instance the carbonation reaction constant, or they depend on the setting considered. Therefore, we first list all parameters in table 3. We give exact values where the parameters are definite and ranges where they are uncertain. The particular values used for the numerical simulations are given in table 4, for the accelerated and natural setting, respectively. Note that due to some dependencies, changing a certain parameter may imply several other changes (e.g. changing $R_{\mathrm{w/c}}$ implies a change in ϕ which, in turn, implies a different u_1^{ext} etc.).

Most of the values of the dimensional parameters can be found in the standard literature, e.g. in [Lid02]. For some specifics, we refer to [BKM03b] and [Ste00], as well as [Arf98] for values of $D_{\mathrm{H_2O}}$.

Parameter	Value	Unit	Description
$R_{\mathrm{w/c}}$	0.4 – 0.6	–	water-to-cement ratio
ϕ_0	0.1 – 0.6	–	initial concrete porosity
ϕ^{a}	0 – 1	–	volume fraction of air-filled pores
ϕ^{w}	0 – 1	–	volume fraction of water-filled pores
L	3	cm	width of the sample
$D_{\mathrm{CO_2}(g)}$	1 – 20	cm^2/day	diffusion constant for $\mathrm{CO_2}(g)$
$D_{\mathrm{CO_2}}$	10^{-6} – 10^{-2}	cm^2/day	diffusion constant for $\mathrm{CO_2}(aq)$
$D_{\mathrm{Ca(OH)_2}}$	10^{-9} – 10^{-5}	cm^2/day	diffusion constant for $\mathrm{Ca(OH)_2}(aq)$
$D_{\mathrm{H_2O}}$	10^{-3} – 10^{-1}	cm^2/day	diffusion constant for moisture
$D_{\mathrm{CaCO_3}}$	0 – 10^{-9}	cm^2/day	diffusion constant for $\mathrm{CaCO_3}(aq)$
C^{Henry}	0.7 – 0.9	–	dimensionless Henry constant
C^{ex}	10^0 – 10^6	1/day	mass transfer coefficient for absorption of $\mathrm{CO_2}(g)$
$C^{\mathrm{Rob}}_{\mathrm{CO_2}(g)}$	1 – 10^5	cm/day	mass transfer coefficient for $\mathrm{CO_2}$ for exchange at the exposed boundary
$C^{\mathrm{Rob}}_{\mathrm{H_2O}}$	1 – 10^7	cm/day	mass transfer coefficient for moisture for exchange at the exposed boundary
C^{reac}	10^5 – 10^8	$\frac{\mathrm{cm}^3}{\mathrm{g}^{p+q}\mathrm{day}}$	carbonation reaction constant
p	1	–	exponent in carbonation reaction rate
q	1	–	exponent in carbonation reaction rate
$m_{\mathrm{CO_2}}$	44	g/mole	molecular weight of $\mathrm{CO_2}$
$m_{\mathrm{Ca(OH)_2}}$	74	g/mole	molecular weight of $\mathrm{Ca(OH)_2}$
$m_{\mathrm{H_2O}}$	18	g/mole	molecular weight of water
$m_{\mathrm{CaCO_3}}$	100	g/mole	molecular weight of $\mathrm{CaCO_3}$
$\phi\phi^{\mathrm{a}}c^0_{\mathrm{CO_2}(g)}$	0	$\mathrm{g/cm}^3$	initial concentration of $\mathrm{CO_2}(g)$
$\phi\phi^{\mathrm{w}}c^0_{\mathrm{CO_2}}$	0	$\mathrm{g/cm}^3$	initial concentration of $\mathrm{CO_2}(aq)$
$\phi\phi^{\mathrm{w}}c^0_{\mathrm{Ca(OH)_2}}$	0.01 – 0.08	$\mathrm{g/cm}^3$	initial concentration of $\mathrm{Ca(OH)_2}(aq)$
ϕw^0	0.02 – 0.04	$\mathrm{g/cm}^3$	initial concentration of moisture
$\phi\phi^{\mathrm{w}}c^0_{\mathrm{CaCO_3}}$	0	$\mathrm{g/cm}^3$	initial concentration of $\mathrm{CaCO_3}$
$c^{\mathrm{ext}}_{\mathrm{CO_2}}$	10^{-3} – 10^{-7}	$\mathrm{g/cm}^3$	ambient concentration of $\mathrm{CO_2}(g)$
ϕw^{ext}	0.02 – 0.04	$\mathrm{g/cm}^3$	ambient concentration of moisture
a	-0.11	–	fitting parameter in sorption isotherm
b	22.7	cm^3/g	fitting parameter in sorption isotherm

Table 3: Values and ranges of dimensional parameters.

Parameter	Accelerated	Natural	Unit
$R_{\mathrm{w/c}}$	0.5	0.6	–
ϕ_0	0.54	0.58	–
ϕ^{a}	0.5	0.5	–
ϕ^{w}	0.5	0.5	–
$D_{\mathrm{CO_2}(g)}$	12	16	$\mathrm{cm}^2/\mathrm{day}$
$D_{\mathrm{CO_2}}$	$1 \cdot 10^{-4}$	$1 \cdot 10^{-4}$	$\mathrm{cm}^2/\mathrm{day}$
$D_{\mathrm{Ca(OH)_2}}$	$1 \cdot 10^{-7}$	$1 \cdot 10^{-7}$	$\mathrm{cm}^2/\mathrm{day}$
$D_{\mathrm{H_2O}}$	$1 \cdot 10^{-2}$	$1 \cdot 10^{-2}$	$\mathrm{cm}^2/\mathrm{day}$
$D_{\mathrm{CaCO_3}}$	0	0	$\mathrm{cm}^2/\mathrm{day}$
C^{Henry}	0.85	0.79	–
C^{ex}	$1 \cdot 10^3$	$5 \cdot 10^3$	1/day
$C^{\mathrm{Rob}}_{\mathrm{CO_2}(g)}$	$1 \cdot 10^5$	$1 \cdot 10^5$	cm/day
$C^{\mathrm{Rob}}_{\mathrm{H_2O}}$	$1 \cdot 10^7$	$1 \cdot 10^7$	cm/day
C^{reac}	461	$1.22 \cdot 10^3$	$\frac{\mathrm{cm}^3}{\mathrm{g}^{p+q}\mathrm{day}}$
$\phi\phi^{\mathrm{w}} c^0_{\mathrm{Ca(OH)_2}}$	0.077	0.077	g/cm^3
ϕw^0	0.033	0.039	g/cm^3
$c^{\mathrm{ext}}_{\mathrm{CO_2}(g)}$	$8.7 \cdot 10^{-4}$	$5.4 \cdot 10^{-7}$	g/cm^3
ϕw^{ext}	0.033	0.039	g/cm^3

Table 4: Specification of the values of table 3 used in the simulations (accelerated and natural carbonation).

References

[ADDN04] D. Agreba-Driollet, F. Diele, and R. Natalini. A mathematical model for the sulfur dioxide aggression to calcium carbonate stones: Numerical approximation and asymptotic analysis. *SIAM Journal on Applied Mathematics*, 64(5):1636–1667, 2004.

[Arf98] J. Arfvidsson. *Moisture Transport in Porous Media. Modelling Based on Kirchhoff Potentials*. PhD thesis, Department of Building Technology, Building Physics, Lund University, 1998. Report TVBH-1010.

[BDJR98] M. Böhm, J. Devinny, F. Jahani, and G. Rosen. On a moving-boundary system modeling corrosion in sewer pipes. *Applied Mathematics and Computation*, 92:247–269, 1998.

[Bie88] Th. A. Bier. *Karbonatisierung und Realkalisierung von Zementstein und Beton*. PhD thesis, University Fridericiana in Karlsruhe, Karlsruhe, 1988. Schriftenreihe des Instituts für Massivbau und Baustofftechnologie. Editors: J. Eibl, H. K. Hilsdorf.

[BKM03a] M. Böhm, J. Kropp, and A. Muntean. A two-reaction-zones moving-interface model for predicting $Ca(OH)_2$-carbonation in concrete. Berichte aus der Technomathematik 03–04, ZeTeM, University of Bremen, 2003.

[BKM03b] M. Böhm, J. Kropp, and A. Muntean. On a prediction model for concrete carbonation based on moving interfaces – interface concentrated reactions. Berichte aus der Technomathematik 03–03, ZeTeM, University of Bremen, 2003.

[BS00] M. Z. Bazant and H. A. Stone. Asymptotics of reaction-diffusion fronts with one static and one diffusing reactant. *Physica D*, 147:95–121, 2000.

[Cha99] T. Chaussadent. États de lieux et réflexions sur la carbonatation du beton armé. Technical report, Laboratoire Central de Ponts et Chaussées, Paris, 1999.

[DL92] R. Dautray and J.-L. Lions. *Evolution Problems I*, volume 5 of *Mathematical analysis and numerical methods for science and technology*. Springer, 1992.

[Do82] D. D. Do. On the validity of the shrinking core model in non-catalytic gas-solid reactions. *Chemical Engineering Science*, 37:1477–1481, 1982.

[Eur98] European Committee for Standardization. *Product and systems for the protection and repair of concrete structures. Test methods. Determination of resistance to carbonation*, 1998. European Standard, prEN 13295.

[FB90] G. F. Froment and K. B. Bischoff. *Chemical Reactor Analysis and Design*. Wiley Series in Chemical Engineering. John Wiley and Sons, 2nd edition, 1990.

[GM03] R. Grotmaack and A. Muntean. Stabilitätsanalyse eines Moving-Boundary-Modells der beschleunigten Karbonatisierung von Portlandzementen. Berichte aus der Technomathematik 03–12, ZeTeM, University of Bremen, 2003.

[Gru97] J. Grunewald. *Diffusiver und konvektiver Stoff- und Energietransport in kapillarporösen Baustoffen*. PhD thesis, Technical University of Dresden, 1997.

[HRW83] Y. Houst, P. Roelfstra, and F. H. Wittmann. A model to predict service life of concrete structures. In *Proc. Int. Conf. Technical Academy Esslingen*, pages 181–186, 1983.

[IM01] T. Ishida and K. Maekawa. Modeling of pH profile in pore water based on mass transport and chemical equilibrium theory. *Concrete Library of JSCE*, 37:131–146, 2001.

[IMS04] T. Ishida, K. Maekawa, and M. Soltani. Theoretically identified strong coupling of carbonation rate and thermodynamic moisture states in micropores of concrete. *Journal of Advanced Concrete Technology*, 2(2):213–222, 2004. Japan Concrete Institute.

[IW68] M. Ishida and C. Y. Wen. Comparison of kinetic and diffusional models for solid-gas reactions. *AIChE J.*, 14(2):311–317, 1968.

[KA00] P. Knabner and L. Angermann. *Numerik partieller Differentialgleichungen. Eine anwendungsorientierte Einführung*. Springer, Berlin, 2000.

[Kro83] J. Kropp. *Karbonatisierung und Transportvorgänge in Zementstein*. PhD thesis, Karlsruhe University, 1983.

[Kro95] J. Kropp. Relations between transport characteristics and durability. In J. Kropp and H. K. Hilsdorf, editors, *Performance Criteria for Concrete Durability*, RILEM Report 12, pages 97–137. E and FN Spon Editions, 1995.

[Lid02] David R. Lide, editor. *CRC Handbook of Chemistry and Physics*. CRC Press LLC, 82 edition, 2001–2002. A Ready-Reference Book of Chemical and Physical Data.

[Mai99] M. Mainguy. Modèles de diffusion non-linéaires en millieux poreux. application à la dissolution et au séchage des matériaux cimentaires. Thése de doctorat, École Nationale des Ponts et Chaussées, Paris, 1999.

[MB04a] A. Muntean and M. Böhm. On a moving reaction layer model for the prediction of the service life of concrete structures. In G. Yagawa, M. Kikuchi, G. M. Atanasiu, and C. Bratianu, editors, *Proceedings of the International Conference Performance based Engineering for 21st Century*, pages 72–77, Iasi, August 2004. Technical University of Iasi, Romania, Cerni Press.

[MB04b] A. Muntean and M. Böhm. On a prediction model for the service life of concrete structures based on moving interfaces. In F. Stangenberg, O. T. Bruhns, D. Hartmann, and G. Meschke, editors, *Proceedings of the Second International Conference Lifetime-Oriented Design Concepts*, pages 209–218, Bochum, March 2004. Ruhr University Bochum, Germany.

[MIK03] K. Maekawa, T. Ishida, and T. Kishi. Multi-scale modeling of concrete performance. integrated material and structural mechanics. *Journal of Advanced Concrete Technology*, 1(2):91–126, 2003. Japan Concrete Institute.

[Mun05] A. Muntean. *Moving Carbonation Models*. PhD thesis, ZeTeM, Departement of Mathematics, University of Bremen, 2005. In preparation.

[NP97] V. T. Ngala and C. L. Page. Effects of carbonation on pore structure and diffusional properties of hydrated cement pastes. *Cement and Concrete Research*, 27(7):995–1007, 1997.

[Ort94] P. J. Ortoleva. *Geochemical Self-Organization*, volume 23 of *Oxford Monographs on Geology and Geophysics*. Oxford University Press, New York, Oxford, 1994.

[PMMB05] M. A. Peter, A. Muntean, S. A. Meier, and M. Böhm. Modelling and simulation of concrete carbonation: competition of several carbonation reactions. Berichte aus der Technomathematik 05-03, ZeTeM, University of Bremen, 2005.

[PVF89] V. G. Papadakis, C. G. Vayenas, and M. N. Fardis. A reaction engineering approach to the problem of concrete carbonation. *AIChE Journal*, 35:1639, 1989.

[PVF91] V. G. Papadakis, C. G. Vayenas, and M. N. Fardis. Fundamental modeling and experimental investigation of concrete carbonation. *ACI Materials Journal*, 88(4):363–373, 1991.

[PVF92] V. G. Papadakis, C. G. Vayenas, and M. N. Fardis. Hydration and carbonation of pozzolanic cements. *ACI Materials Journal*, 89(2):119–130, 1992.

[SDA02] A. Steffens, D. Dinkler, and H. Ahrens. Modeling carbonation for corrosion risk prediction of concrete structures. *Cement and Concrete Research*, 32:935–941, 2002.

[SES76] J. Szekely, J. W. Evans, and H. Y. Sohn. *Gas-Solid Reactions*. Academic Press, 1976.

[SGS04] A. M. Soane, M. K. Gobbert, and T. Seidman. Design on an effective numerical method for a reaction-diffusion system with internal and transient layers. Technical report, Institute of Mathematics and its Applications, Minneapolis, Minnesota, November 2004.

[SGS05] A. M. Soane, M. K. Gobbert, and T. Seidman. Numerical exploration of a system of reaction-diffusion equations with internal and transient layers. *Nonlinear Analysis: Real World Applications*, 2005. in press.

[Sis04] K. Sisomphon. *Influence of Pozzolanic Material Additions on the Development of the Alkalinity and the Carbonation Behaviour of Composite Cement Pastes and Concretes*. PhD thesis, TU Hamburg-Harburg, 2004.

[SMB99] E. Samson, J. Marchand, and J. J. Beaudoin. Describing ion diffusion in cement-based materials using the homogenization technique. *Cement and Concrete Research*, 29:1341–1345, 1999.

[SMB05] A. Schmidt, A. Muntean, and M. Böhm. Numerical experiments with self-adaptive finite element simulations in 2D for the carbonation of concrete. Berichte aus der Technomathematik 05-01, ZeTeM, University of Bremen, 2005.

[SN97] T. Saeki and S. Nagataki. Effect of hydration of cement after initial curing on carbonation rate. In *International Conference on Engineering Materials*, pages 315–329, June 1997.

[SON90] T. Saeki, H. Ohga, and S. Nagataki. Change in micro-structure of concrete due to carbonation. *Concrete Library of JSCE*, 420(V-13):1–12, 1990.

[SSV93] A. V. Saetta, B. A. Schrefler, and R. V. Vitaliani. The carbonation of concrete and the mechanism of moisture, heat and carbon dioxide flow through porous materials. *Cement and Concrete Research*, 23(4):761–772, 1993.

[SSV95] A. V. Saetta, B. A. Schrefler, and R. V. Vitaliani. 2D model for carbonation and moisture/heat flow in porous materials. *Cement and Concrete Research*, 25(8):1703–1712, 1995.

[Ste00] A. Steffens. *Modellierung von Karbonatisierung und Chloridbindung zur numerischen Analyse der Korrosionsgefährdung der Betonbewehrung*. PhD thesis, Institute for Statics, Technical University Braunschweig, 2000.

[SV04] A. V. Saetta and R. V. Vitaliani. Experimental investigation and numerical modeling of carbonation process in reinforced concrete structures. Part I: Theoretical formulation. *Cement and Concrete Research*, 34(4):571–579, 2004.

[Tay97] H. F. W. Taylor. *Cement Chemistry*. Thomas Telford Publishing, London, 1997.

[TM03] R. Tixier and B. Mobasher. Modeling of damage in cement-based materials subjected to external sulfate attack. I.: Formulation. *Journal of Materials in Civil Engineering, ASCE Publications*, 15(4):305–313, 2003.

[WD96] W. A. Weber and F. A. DiGiano. *Process Dynamics in Environmental Systems*. Environmental Science and Technology. John Wiley and Sons, Inc., 1996.

[Wie84] H.-J. Wierig. Longtime studies on the carbonation of concrete under normal outdoor exposure. In *Proceedings of the RILEM, Hannover University*, pages 239–249. RILEM, 1984.

Berichte aus der Technomathematik ISSN 1435-7968

http://www.math.uni-bremen.de/zetem/berichte.html

— Vertrieb durch den Autor —

Reports **Stand: 20. April 2005**

98–01. Peter Benner, Heike Faßbender:
An Implicitly Restarted Symplectic Lanczos Method for the Symplectic Eigenvalue Problem, Juli 1998.

98–02. Heike Faßbender:
Sliding Window Schemes for Discrete Least-Squares Approximation by Trigonometric Polynomials, Juli 1998.

98–03. Peter Benner, Maribel Castillo, Enrique S. Quintana-Ortí:
Parallel Partial Stabilizing Algorithms for Large Linear Control Systems, Juli 1998.

98–04. Peter Benner:
Computational Methods for Linear–Quadratic Optimization, August 1998.

98–05. Peter Benner, Ralph Byers, Enrique S. Quintana-Ortí, Gregorio Quintana-Ortí:
Solving Algebraic Riccati Equations on Parallel Computers Using Newton's Method with Exact Line Search, August 1998.

98–06. Lars Grüne, Fabian Wirth:
On the rate of convergence of infinite horizon discounted optimal value functions, November 1998.

98–07. Peter Benner, Volker Mehrmann, Hongguo Xu:
A Note on the Numerical Solution of Complex Hamiltonian and Skew-Hamiltonian Eigenvalue Problems, November 1998.

98–08. Eberhard Bänsch, Burkhard Höhn:
Numerical simulation of a silicon floating zone with a free capillary surface, Dezember 1998.

99–01. Heike Faßbender:
The Parameterized SR Algorithm for Symplectic (Butterfly) Matrices, Februar 1999.

99–02. Heike Faßbender:
Error Analysis of the symplectic Lanczos Method for the symplectic Eigenvalue Problem, März 1999.

99–03. Eberhard Bänsch, Alfred Schmidt:
Simulation of dendritic crystal growth with thermal convection, März 1999.

99–04. Eberhard Bänsch:
Finite element discretization of the Navier-Stokes equations with a free capillary surface, März 1999.

99–05. Peter Benner:
Mathematik in der Berufspraxis, Juli 1999.

99–06. Andrew D.B. Paice, Fabian R. Wirth:
Robustness of nonlinear systems and their domains of attraction, August 1999.

99–07. Peter Benner, Enrique S. Quintana-Ortí, Gregorio Quintana-Ortí:
Balanced Truncation Model Reduction of Large-Scale Dense Systems on Parallel Computers, September 1999.

99–08. Ronald Stöver:
Collocation methods for solving linear differential-algebraic boundary value problems, September 1999.

99–09. Huseyin Akcay:
Modelling with Orthonormal Basis Functions, September 1999.

99–10. Heike Faßbender, D. Steven Mackey, Niloufer Mackey:
Hamilton and Jacobi come full circle: Jacobi algorithms for structured Hamiltonian eigenproblems, Oktober 1999.

99–11. Peter Benner, Vincente Hernández, Antonio Pastor:
On the Kleinman Iteration for Nonstabilizable System, Oktober 1999.

99–12. Peter Benner, Heike Faßbender:
A Hybrid Method for the Numerical Solution of Discrete-Time Algebraic Riccati Equations, November 1999.

99–13. Peter Benner, Enrique S. Quintana-Ortí, Gregorio Quintana-Ortí:
Numerical Solution of Schur Stable Linear Matrix Equations on Multicomputers, November 1999.

99–14. Eberhard Bänsch, Karol Mikula:
Adaptivity in 3D Image Processing, Dezember 1999.

00–01. Peter Benner, Volker Mehrmann, Hongguo Xu:
Perturbation Analysis for the Eigenvalue Problem of a Formal Product of Matrices, Januar 2000.

00–02. Ziping Huang:
Finite Element Method for Mixed Problems with Penalty, Januar 2000.

00–03. Gianfrancesco Martinico:
Recursive mesh refinement in 3D, Februar 2000.

00–04. Eberhard Bänsch, Christoph Egbers, Oliver Meincke, Nicoleta Scurtu:
Taylor-Couette System with Asymmetric Boundary Conditions, Februar 2000.

00–05. Peter Benner:
Symplectic Balancing of Hamiltonian Matrices, Februar 2000.

00–06. Fabio Camilli, Lars Grüne, Fabian Wirth:
A regularization of Zubov's equation for robust domains of attraction, März 2000.

00–07. Michael Wolff, Eberhard Bänsch, Michael Böhm, Dominic Davis:
Modellierung der Abkühlung von Stahlbrammen, März 2000.

00–08. Stephan Dahlke, Peter Maaß, Gerd Teschke:
Interpolating Scaling Functions with Duals, April 2000.

00–09. Jochen Behrens, Fabian Wirth:
A globalization procedure for locally stabilizing controllers, Mai 2000.

00–10. Peter Maaß, Gerd Teschke, Werner Willmann, Günter Wollmann:
Detection and Classification of Material Attributes – A Practical Application of Wavelet Analysis, Mai 2000.

00–11. Stefan Boschert, Alfred Schmidt, Kunibert G. Siebert, Eberhard Bänsch, Klaus-Werner Benz, Gerhard Dziuk, Thomas Kaiser:
Simulation of Industrial Crystal Growth by the Vertical Bridgman Method, Mai 2000.

00–12. Volker Lehmann, Gerd Teschke:
Wavelet Based Methods for Improved Wind Profiler Signal Processing, Mai 2000.

00–13. Stephan Dahlke, Peter Maass:
A Note on Interpolating Scaling Functions, August 2000.

00–14. Ronny Ramlau, Rolf Clackdoyle, Frédéric Noo, Girish Bal:
Accurate Attenuation Correction in SPECT Imaging using Optimization of Bilinear Functions and Assuming an Unknown Spatially-Varying Attenuation Distribution, September 2000.

00–15. Peter Kunkel, Ronald Stöver:
Symmetric collocation methods for linear differential-algebraic boundary value problems, September 2000.

00–16. Fabian Wirth:
The generalized spectral radius and extremal norms, Oktober 2000.

00–17. Frank Stenger, Ahmad Reza Naghsh-Nilchi, Jenny Niebsch, Ronny Ramlau:
A unified approach to the approximate solution of PDE, November 2000.

00–18. Peter Benner, Enrique S. Quintana-Ortí, Gregorio Quintana-Ortí:
Parallel algorithms for model reduction of discrete–time systems, Dezember 2000.

00–19. Ronny Ramlau:
A steepest descent algorithm for the global minimization of Tikhonov–Phillips functional, Dezember 2000.

01–01. Efficient methods in hyperthermia treatment planning:
Torsten Köhler, Peter Maass, Peter Wust, Martin Seebass, Januar 2001.

01–02. Parallel Algorithms for LQ Optimal Control of Discrete-Time Periodic Linear Systems:
Peter Benner, Ralph Byers, Rafael Mayo, Enrique S. Quintana-Ortí, Vicente Hernández, Februar 2001.

01–03. Peter Benner, Enrique S. Quintana-Ortí, Gregorio Quintana-Ortí:
Efficient Numerical Algorithms for Balanced Stochastic Truncation, März 2001.

01–04. Peter Benner, Maribel Castillo, Enrique S. Quintana-Ortí:
Partial Stabilization of Large-Scale Discrete-Time Linear Control Systems, März 2001.

01–05. Stephan Dahlke:
Besov Regularity for Edge Singularities in Polyhedral Domains, Mai 2001.

01–06. Fabian Wirth:
A linearization principle for robustness with respect to time-varying perturbations, Mai 2001.

01–07. Stephan Dahlke, Wolfgang Dahmen, Karsten Urban:
Adaptive Wavelet Methods for Saddle Point Problems - Optimal Convergence Rates, Juli 2001.

01–08. Ronny Ramlau:
Morozov's Discrepancy Principle for Tikhonov regularization of nonlinear operators, Juli 2001.

01–09. Michael Wolff:
Einführung des Drucks für die instationären Stokes–Gleichungen mittels der Methode von Kaplan, Juli 2001.

01–10. Stephan Dahlke, Peter Maaß, Gerd Teschke:
Reconstruction of Reflectivity Desities by Wavelet Transforms, August 2001.

01–11. Stephan Dahlke:
Besov Regularity for the Neumann Problem, August 2001.

01–12. Bernard Haasdonk, Mario Ohlberger, Martin Rumpf, Alfred Schmidt, Kunibert G. Siebert:
h–p–Multiresolution Visualization of Adaptive Finite Element Simulations, Oktober 2001.

01–13. Stephan Dahlke, Gabriele Steidl, Gerd Teschke:
Coorbit Spaces and Banach Frames on Homogeneous Spaces with Applications to Analyzing Functions on Spheres, August 2001.

02–01. Michael Wolff, Michael Böhm:
Zur Modellierung der Thermoelasto-Plastizität mit Phasenumwandlungen bei Stählen sowie der Umwandlungsplastizität, Februar 2002.

02–02. Stephan Dahlke, Peter Maaß:
An Outline of Adaptive Wavelet Galerkin Methods for Tikhonov Regularization of Inverse Parabolic Problems, April 2002.

02–03. Alfred Schmidt:
A Multi-Mesh Finite Element Method for Phase Field Simulations, April 2002.

02–04. Sergey N. Dachkovski, Michael Böhm:
A Note on Finite Thermoplasticity with Phase Changes, Juli 2002.

02–05. Michael Wolff, Michael Böhm:
Phasenumwandlungen und Umwandlungsplastizität bei Stählen im Konzept der Thermoelasto-Plastizität, Juli 2002.

02–06. Gerd Teschke:
Construction of Generalized Uncertainty Principles and Wavelets in Anisotropic Sobolev Spaces, August 2002.

02–07. Ronny Ramlau:
TIGRA – an iterative algorithm for regularizing nonlinear ill–posed problems, August 2002.

02–08. Michael Lukaschewitsch, Peter Maaß, Michael Pidcock:
Tikhonov regularization for Electrical Impedance Tomography on unbounded domains, Oktober 2002.

02–09. Volker Dicken, Peter Maaß, Ingo Menz, Jenny Niebsch, Ronny Ramlau:
Inverse Unwuchtidentifikation an Flugtriebwerken mit Quetschöldämpfern, Oktober 2002.

02–10. Torsten Köhler, Peter Maaß, Jan Kalden:
Time-series forecasting for total volume data and charge back data, November 2002.

02–11. Angelika Bunse-Gerstner:
A Short Introduction to Iterative Methods for Large Linear Systems, November 2002.

02–12. Peter Kunkel, Volker Mehrmann, Ronald Stöver:
Symmetric Collocation for Unstructured Nonlinear Differential-Algebraic Equations of Arbitrary Index, November 2002.

02–13. Michael Wolff:
Ringvorlesung: Distortion Engineering 2
Kontinuumsmechanische Modellierung des Materialverhaltens von Stahl unter Berücksichtigung von Phasenumwandlungen, Dezember 2002.

02–14. Michael Böhm, Martin Hunkel, Alfred Schmidt, Michael Wolff:
Evaluation of various phase-transition models for 100Cr6 for application in commercial FEM programs, Dezember 2002.

03–01. Michael Wolff, Michael Böhm, Serguei Dachkovski:
Volumenanteile versus Massenanteile - der Dilatometerversuch aus der Sicht der Kontinuumsmechanik, Januar 2003.

03–02. Daniel Kessler, Ricardo H. Nochetto, Alfred Schmidt:
A posteriori error control for the Allen-Cahn Problem: circumventing Gronwall's inequality, März 2003.

03–03. Michael Böhm, Jörg Kropp, Adrian Muntean:
On a Prediction Model for Concrete Carbonation based on Moving Interfaces - Interface concentrated Reactions, April 2003.

03–04. Michael Böhm, Jörg Kropp, Adrian Muntean:
A Two-Reaction-Zones Moving-Interface Model for Predicting $Ca(OH)_2$ Carbonation in Concrete, April 2003.

03–05. Vladimir L. Kharitonov, Diederich Hinrichsen:
Exponential estimates for time delay systems, May 2003.

03–06. Michael Wolff, Michael Böhm, Serguei Dachkovski, Günther Löwisch:
Zur makroskopischen Modellierung von spannungsabhängigem Umwandlungsverhalten und Umwandlungsplastizität bei Stählen und ihrer experimentellen Untersuchung in einfachen Versuchen, Juli 2003.

03–07. Serguei Dachkovski, Michael Böhm, Alfred Schmidt, Michael Wolff:
Comparison of several kinetic equations for pearlite transformation in 100Cr6 steel,
Juli 2003.

03–08. Volker Dicken, Peter Maass, Ingo Menz, Jenny Niebsch, Ronny Ramlau:
Nonlinear Inverse Unbalance Reconstruction in Rotor dynamics,
Juli 2003.

03–09. Michael Böhm, Serguei Dachkovski, Martin Hunkel, Thomas Lübben, Michael Wolff:
Übersicht über einige makroskopische Modelle für Phasenumwandlungen im Stahl,
Juli 2003.

03–10. Michael Wolff, Friedhelm Frerichs, Bettina Suhr:
Vorstudie für einen Bauteilversuch zur Umwandlungsplastizität bei der perlitischen Umwandlung des Stahls 100 Cr6,
August 2003.

03–11. Michael Wolff, Bettina Suhr:
Zum Vergleich von Massen- und Volumenanteilen bei der perlitischen Umwandlung der Stähle 100Cr6 und C80,
September 2003.

03–12. Rike Grotmaack, Adrian Muntean:
Stabilitätsanalyse eines Moving-Boundary-Modells der beschleunigten Karbonatisierung von Portlandzementen,
September 2003.

03–13. Alfred Schmidt, Michael Wolff, Michael Böhm:
Numerische Untersuchungen für ein Modell des Materialverhaltens mit Umwandlungsplastizität und Phasenumwandlungen beim Stahl 100Cr6 (Teil 1),
September 2003.

04–01. Liliana Cruz Martin, Gerd Teschke:
A new method to reconstruct radar reflectivities and Doppler information,
Januar 2004.

04–02. Ingrid Daubechies, Gerd Teschke:
Wavelet based image decomposition by variational functionals,
Januar 2004.

04–03. N. Guglielmi, F. Wirth, M. Zennaro:
Complex polytope extremality results for families of matrices,
März 2004.

04–04. I. Daubechies, G. Teschke:
Variational image restoration by means of wavelets: simultaneous decomposition, deblurring and denoising,
April 2004.

04–05. V.L. Kharitonov, E. Plischke:
Lyapunov matrices for time-delay systems,
April 2004.

04–06. Ronny Ramlau:
On the use of fixed point iterations for the regularization of nonlinear ill-posed problems,
Juni 2004.

04–07. Christof Büskens, Matthias Knauer:
Higher Order Real-Time Approximations In Optimal Control of Multibody-Systems For Industrial Robots,
August 2004.

04–08. Christof Büskens, Roland Griesse:
Computational Parametric Sensitivity Analysis of Perturbed PDE Optimal Control Problems with State and Control Constraints,
August 2004.

04–09. Christof Büskens:
Higher Order Real-Time Approximations of Perturbed Control Constrainted PDE Optimal Control Problems ,
August 2004.

04–10. Christof Büskens, Matthias Gerdts:
Differentiability of Consistency Functions,
August 2004.

04–11. Robert Baier, Christof Büskens, Ilyes Aïssa Chama, Matthias Gerdts:
Approximation of Reachable Sets by Direct Solution Methods of Optimal Control Problems,
August 2004.

04–12. J. Soares, G. Teschke, M. Zhariy:
A Wavelet Regularization for Nonlinear Diffusion Equations,
September 2004.

05–01. Alfred Schmidt, Adrian Muntean, Michael Böhm:
Numerical experiments with Self-Adaptive Finite Element Simulations in 2D for the Carbonation of Concrete,
April 2005.

05–02. Sebastian A. Meier, Malte A. Peter, Adrian Muntean, Michael Böhm:
Modelling and simulation of concrete carbonation with internal layers,
April 2005.